2017

光物性物理学

Optical Properties and Spectroscopy of Materials

松田巌

Lecture Note 2

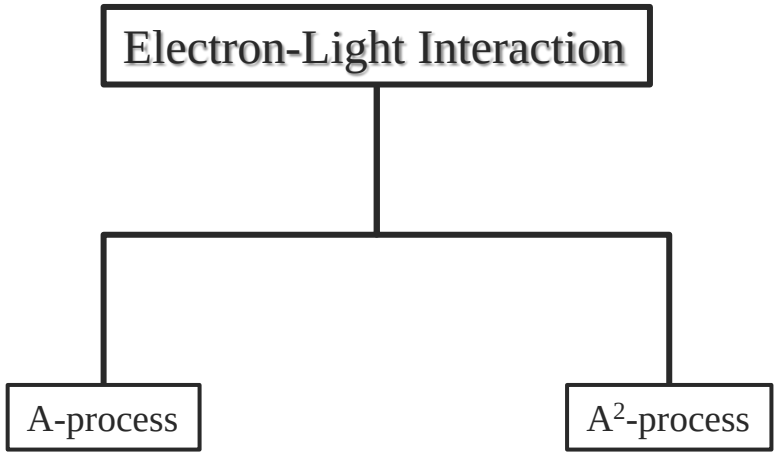
Electron-Light Interaction
A-process
A^2-process

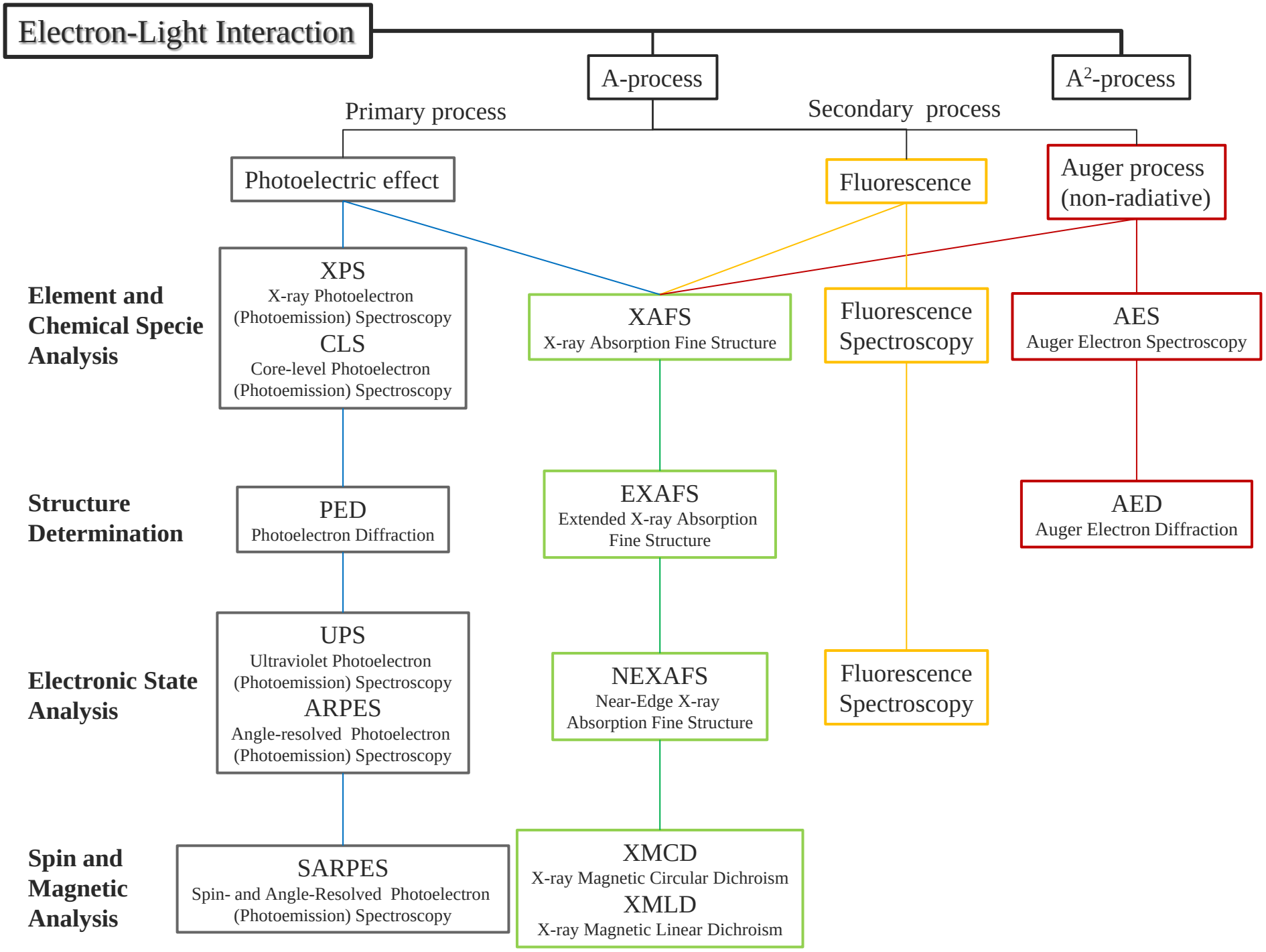
Electron-Light Interaction
A-process
A²-process
Primary process
Secondary process
Photoelectric effect
Fluorescence
Auger process (non-radiative)
Element and Chemical Specie Analysis
XPS
X-ray Photoelectron (Photoemission) Spectroscopy
CLS
Core-level Photoelectron (Photoemission) Spectroscopy
XAFS
X-ray Absorption Fine Structure
Fluorescence Spectroscopy
AES
Auger Electron Spectroscopy
Structure Determination
PED
Photoelectron Diffraction
EXAFS
Extended X-ray Absorption Fine Structure
AED
Auger Electron Diffraction
Electronic State Analysis
UPS
Ultraviolet Photoelectron (Photoemission) Spectroscopy
ARPES
Angle-resolved Photoelectron (Photoemission) Spectroscopy
NEXAFS
Near-Edge X-ray Absorption Fine Structure
Fluorescence Spectroscopy
Spin and Magnetic Analysis
SARPES
Spin- and Angle-Resolved Photoelectron (Photoemission) Spectroscopy
XMCD
X-ray Magnetic Circular Dichroism
XMLD
X-ray Magnetic Linear Dichroism

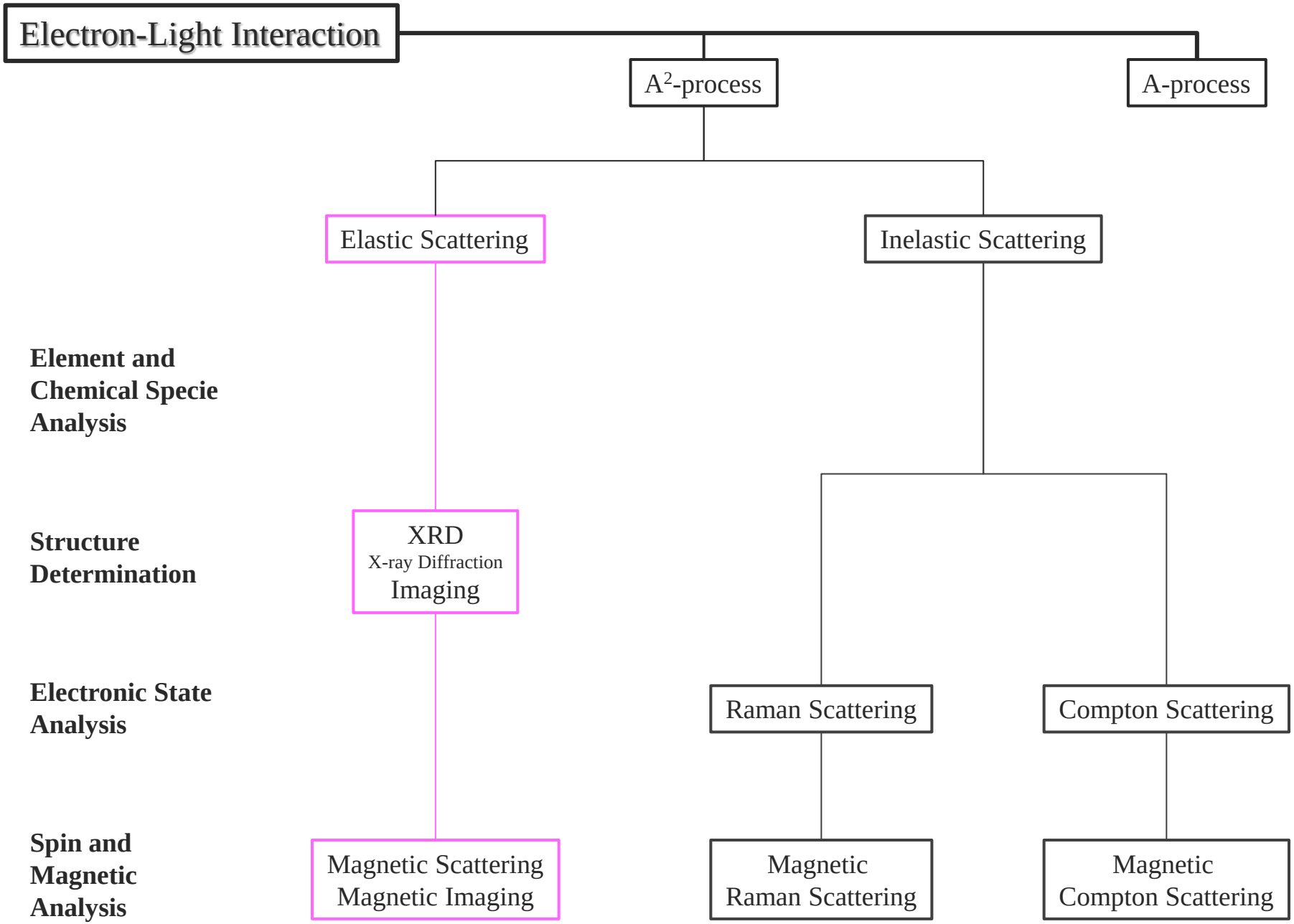
Electron-Light Interaction
A2-process
A-process
Elastic Scattering
Inelastic Scattering
Element and Chemical Specie Analysis
Structure Determination
XRD
X-ray Diffraction
Imaging
Electronic State Analysis
Raman Scattering
Compton Scattering
Spin and Magnetic Analysis
Magnetic Scattering
Magnetic Imaging
Magnetic
Raman Scattering
Magnetic
Compton Scattering

Probing electronic states

- Photoelectron spectroscopy

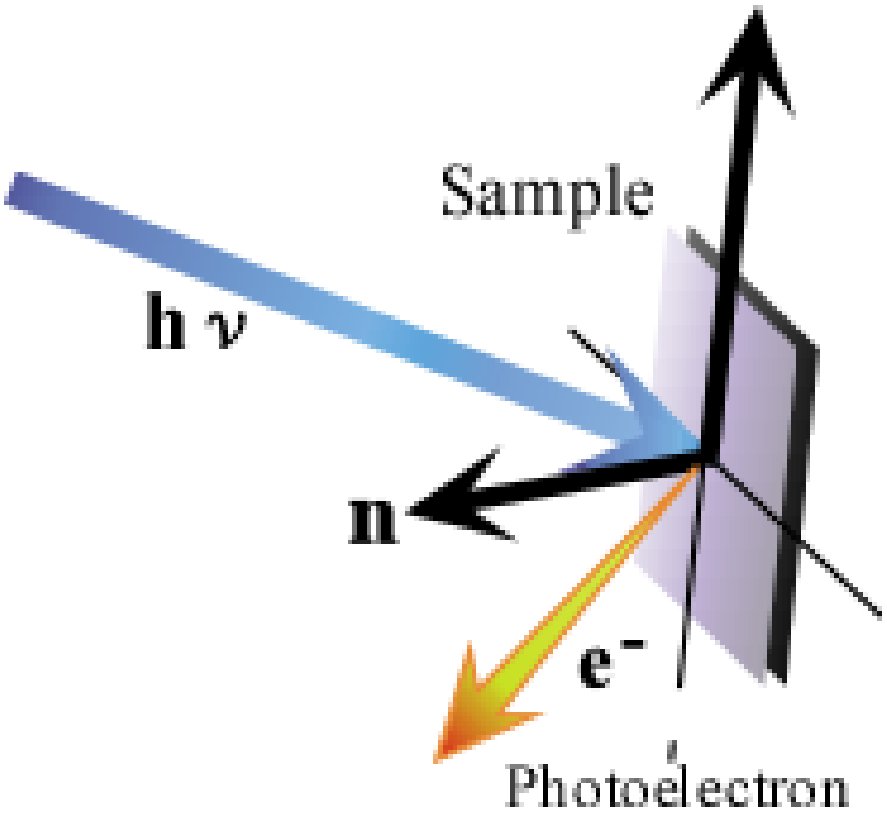

電子

分子

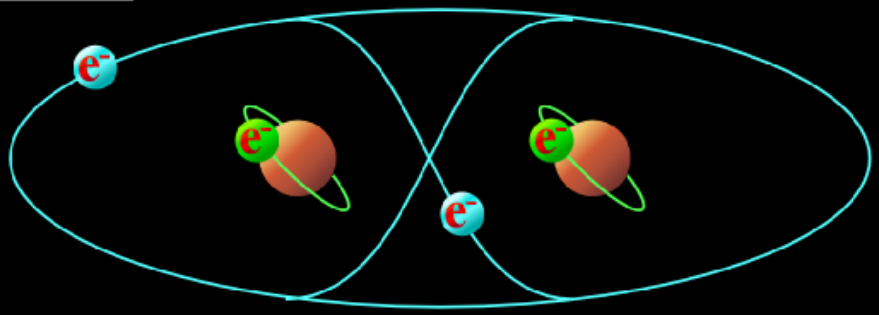

原子

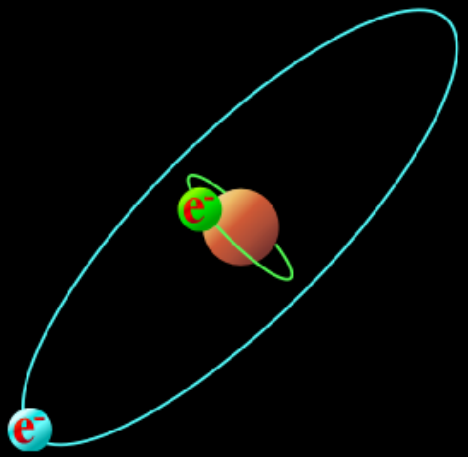

固体

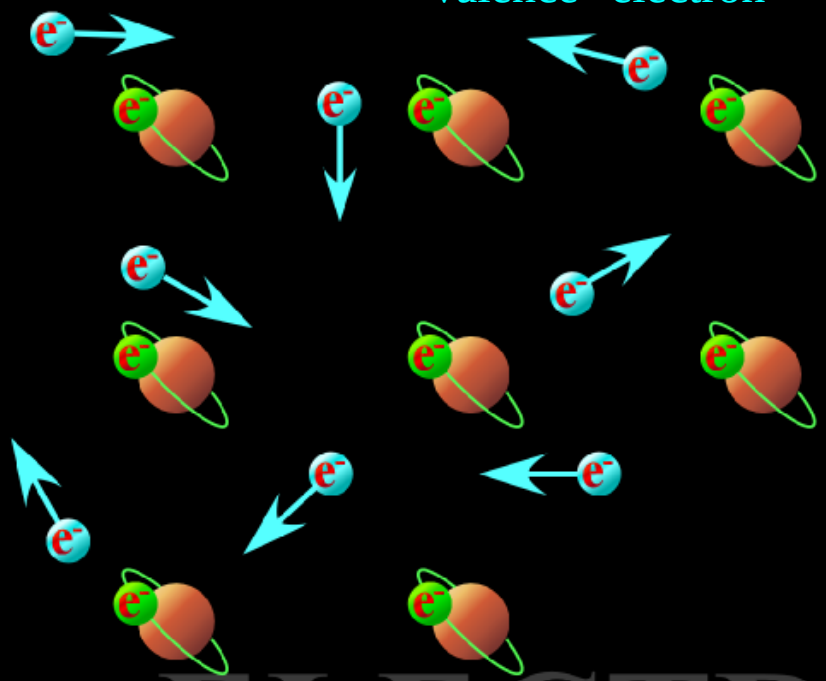

ELECTRON

What can be probed by photoemission

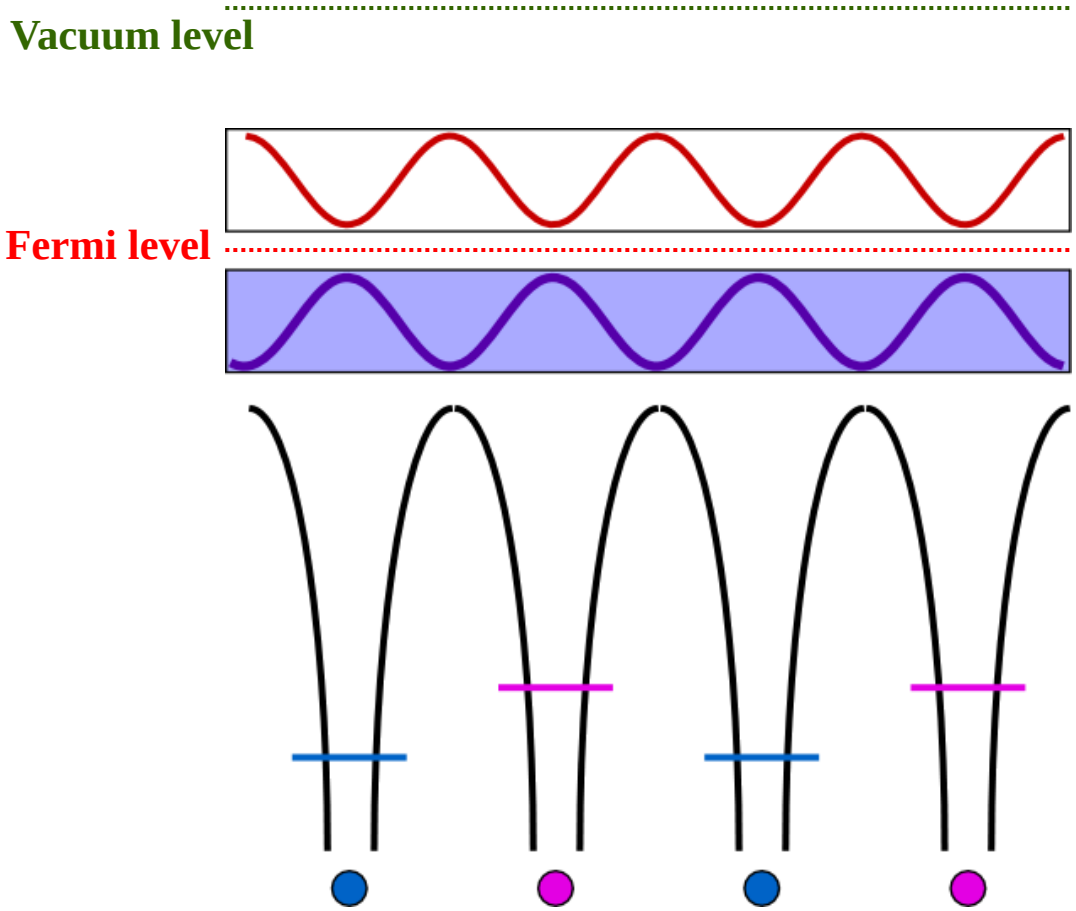

Band Dispersions of
- partially occupied states (metal)
- fully occupied states (semiconductor)

Energy shift of core-levels
- Different elements
- Different chemical sites (environments)

Probing electronic states

- Photoelectron spectroscopy

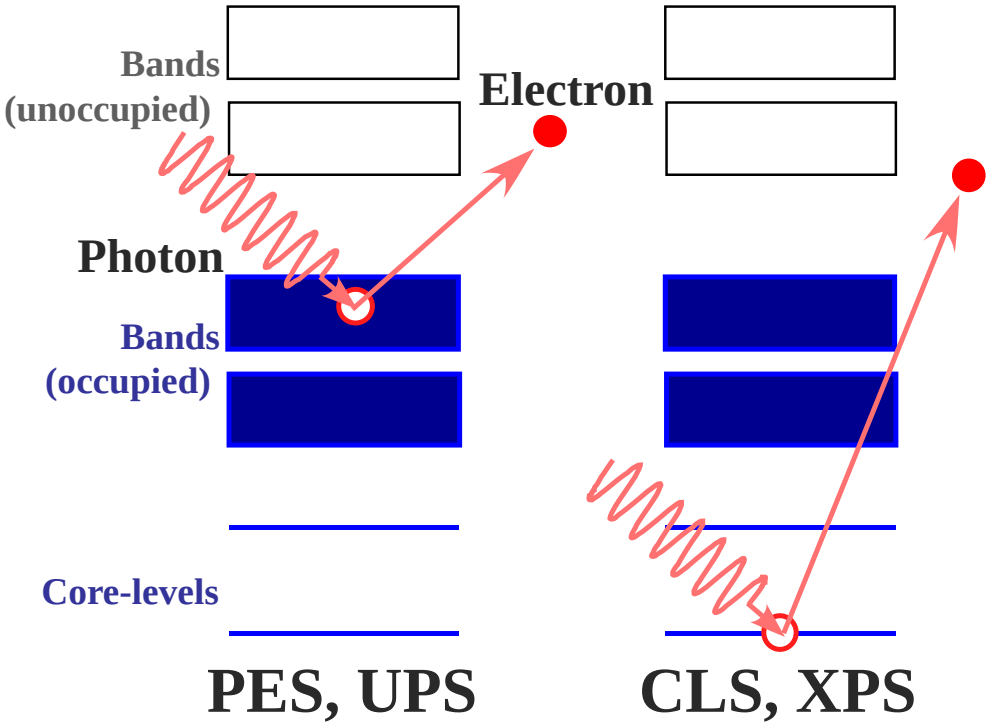

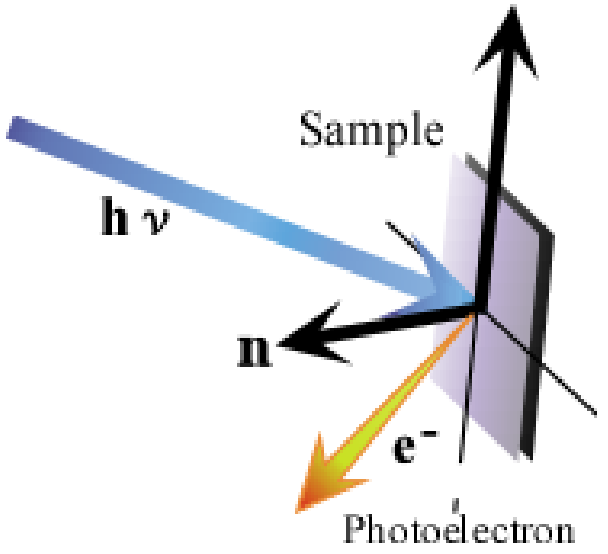

$$E_k = h\nu - \Phi - E_B$$

work function — binding energy

Probing electronic states

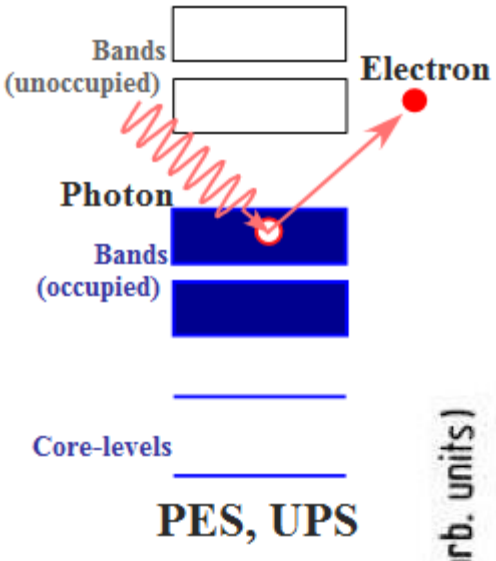

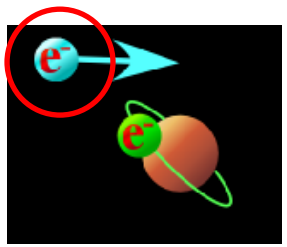

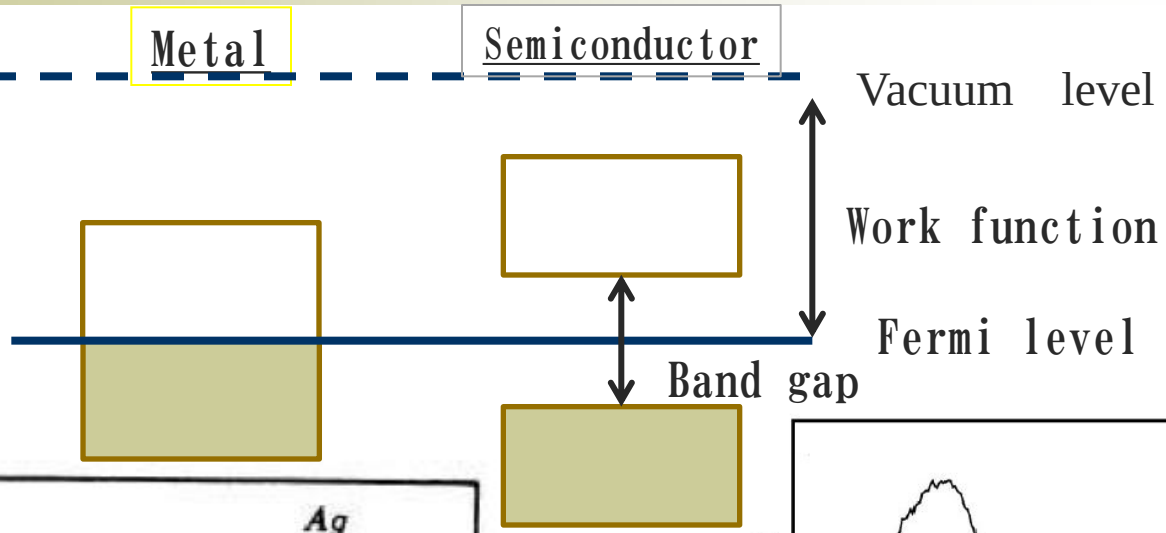

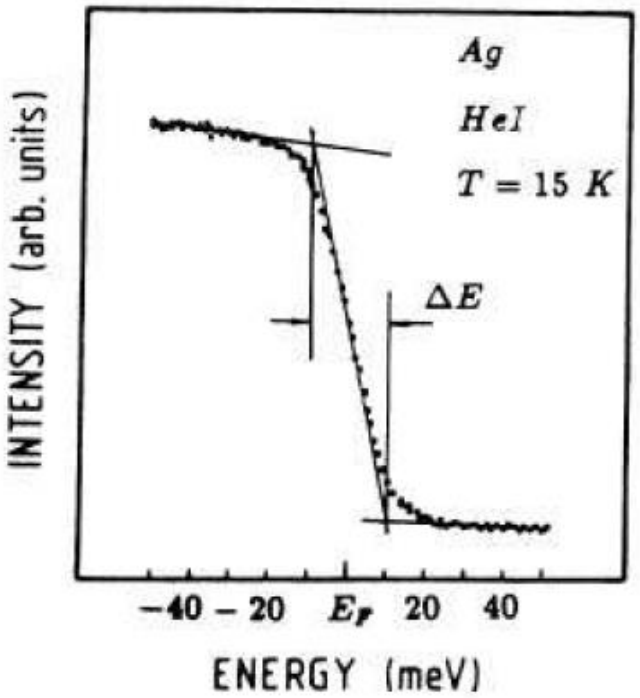

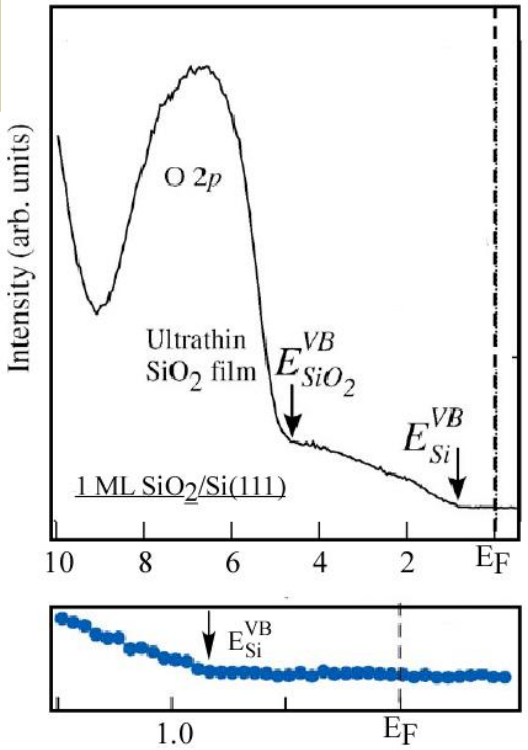

Probing electronic states

CLS, XPS
ESCA (Electron Spectroscopy for Chemical Analysis)

Chemical shifts

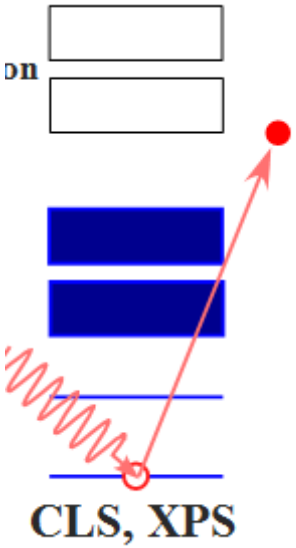

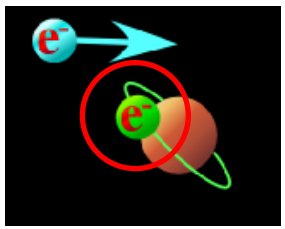

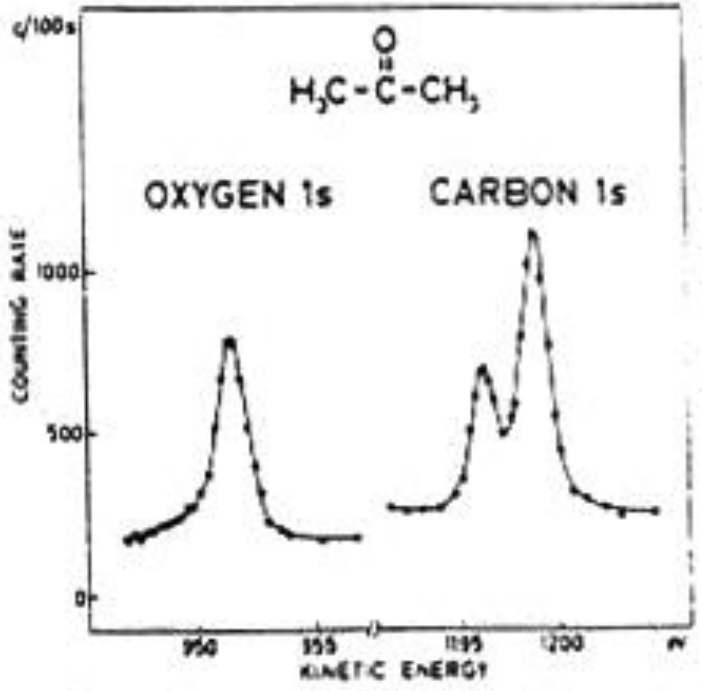

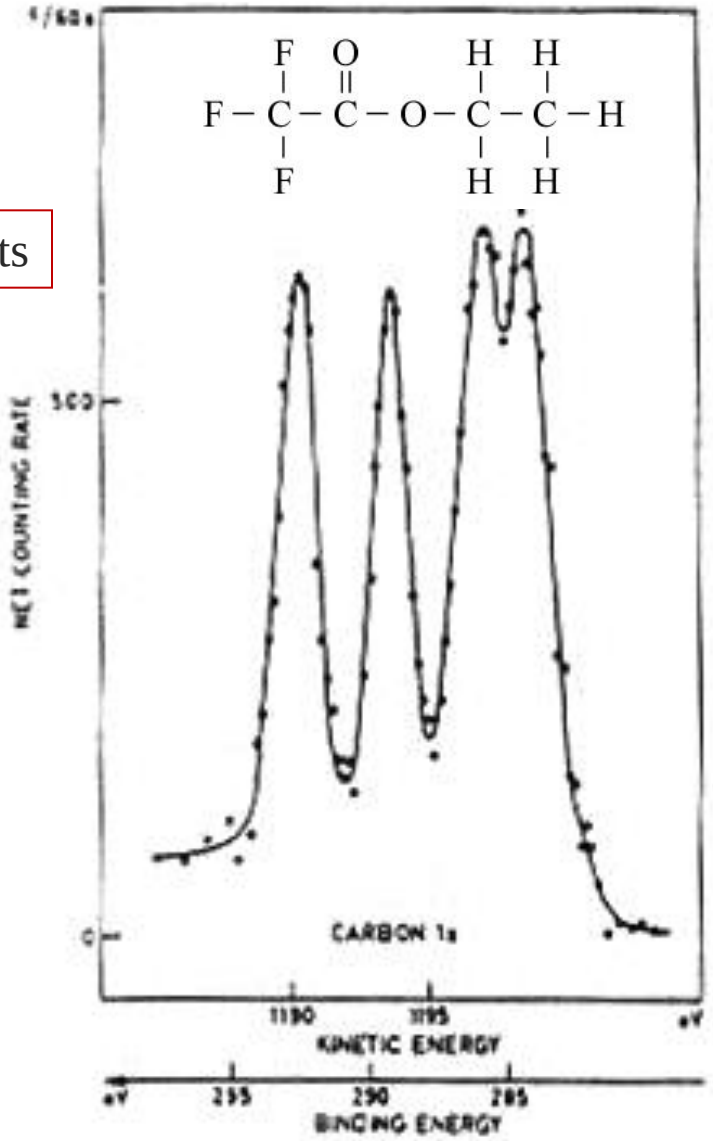

Principle

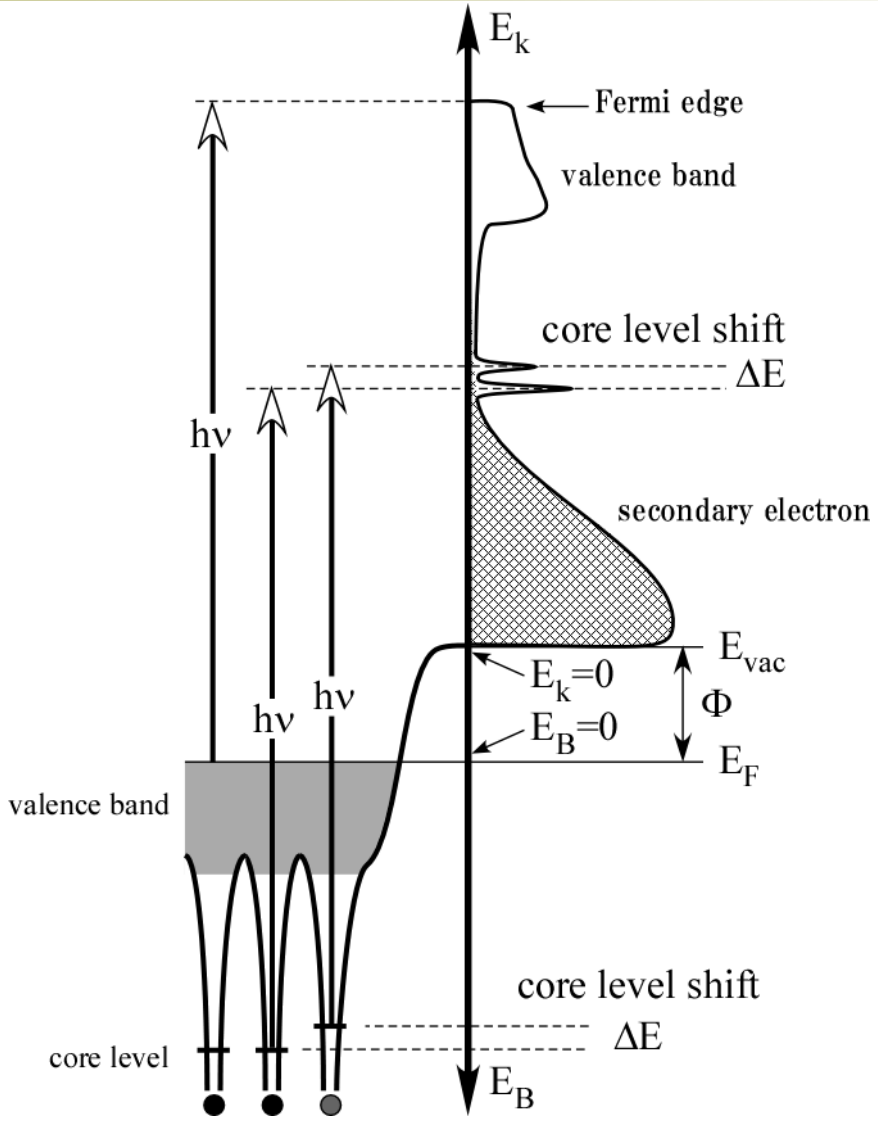
E_k
Fermi edge
valence band
core level shift
ΔE
hν
secondary electron
E_vac
E_k=0
Φ
hν
hν
E_B=0
E_F
valence band
core level shift
ΔE
core level
E_B

Three step model

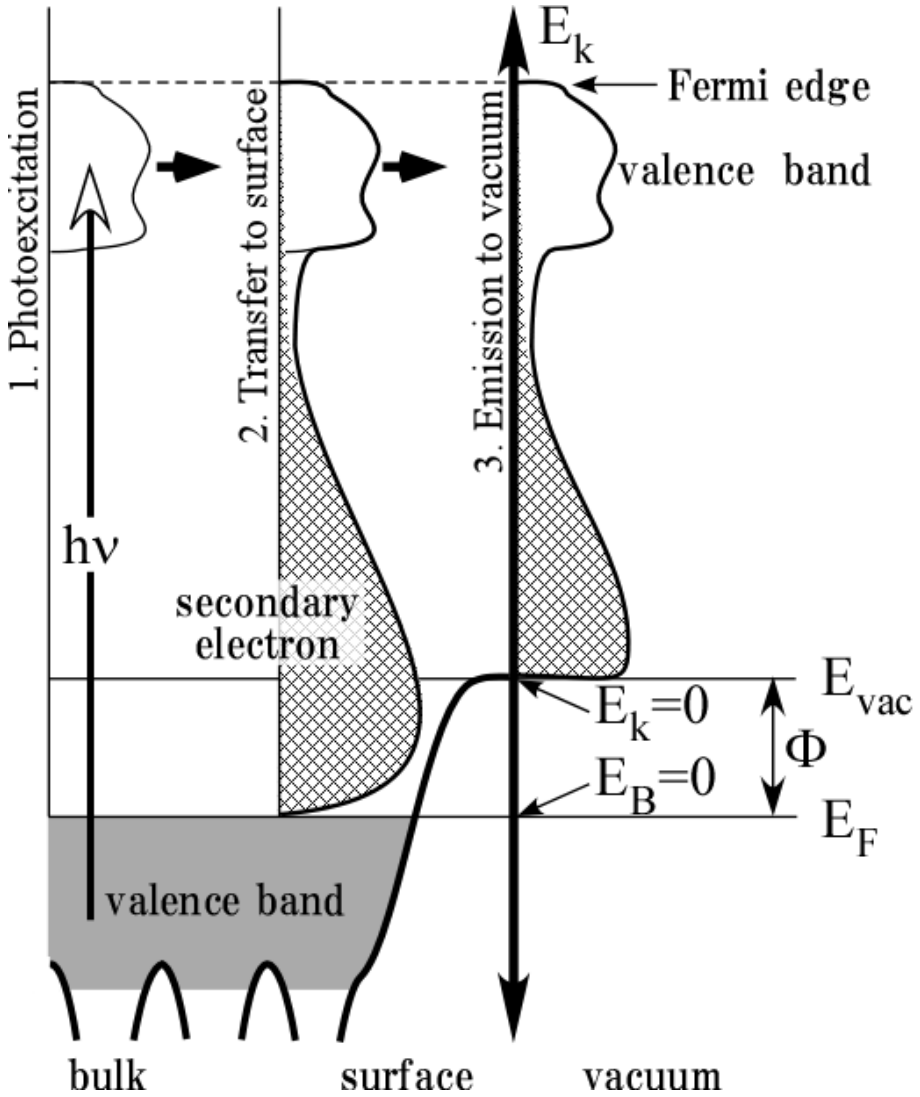

Electron Kinetic Energy in vacuum (eV)

$$E_k = h\nu - \Phi - E_B$$

work function — binding energy

$$k_{\parallel}(\text{Å}^{-1}) = 0.512\ \{(h\nu-\Phi-E_B)\}^{1/2} \cdot \sin\theta_e$$

$$k_{z,in} = \sqrt{k_{z,out}^2 + (0.512)^2 V_0}$$

Vo: inner potential

Electron escape depth

- The universal curve

A. Zangwill, Physics at Surface

surface-sensitive ~ bulk sensitive

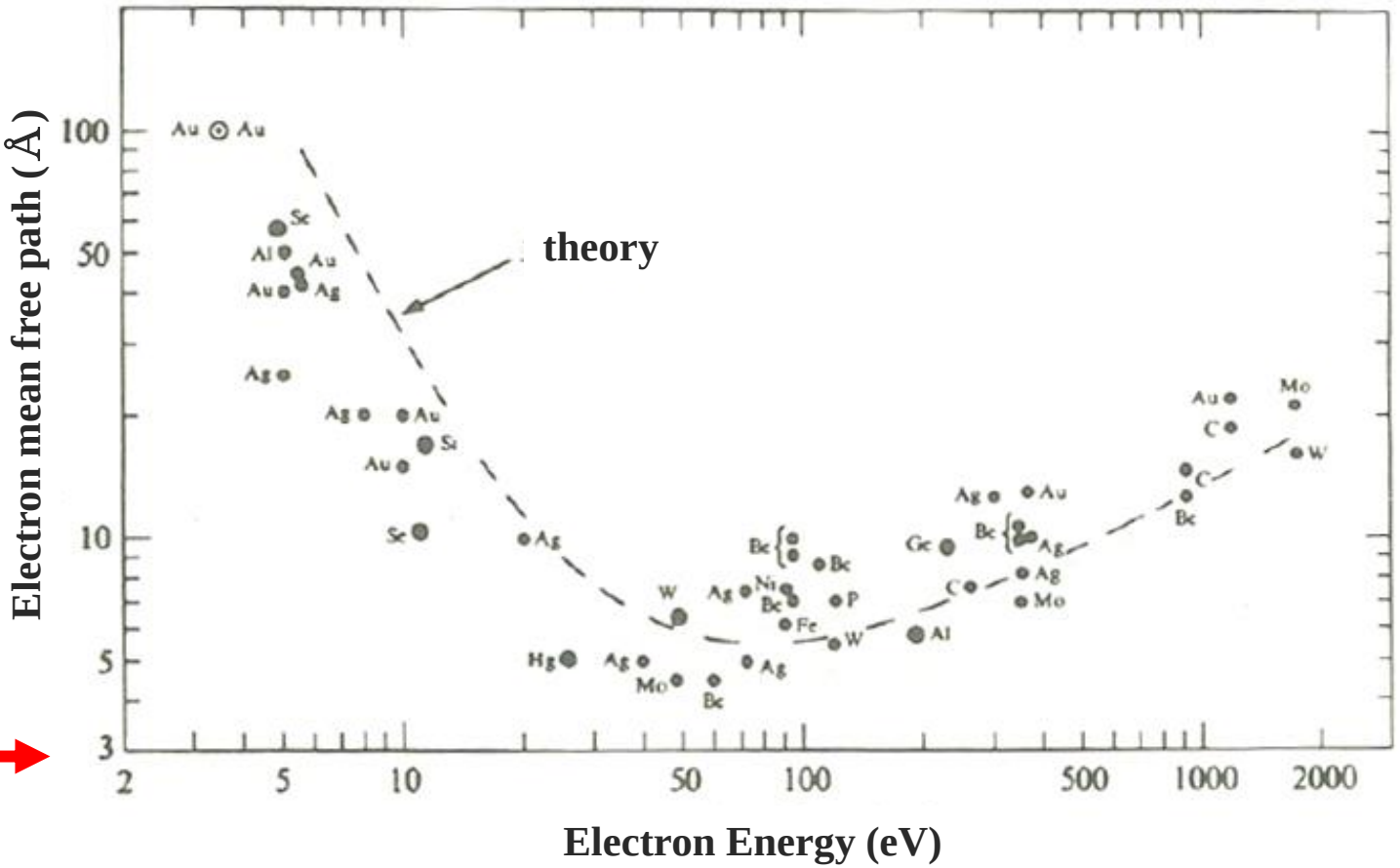

Atomic layer

Fermiology

Transport, Magnetism, Superconductivity, Transition, and etc of Metal are determined by the Fermi surface

Understanding metal => determining Fermi surface (Fermiology)

- Photoemission Fermi surface mapping

Periodic Table of the Fermi Surfaces of Elemental Solids

http://www.phys.ufl.edu/fermisurface

Tat-Sang Choy, Jeffery Naset , Selman Hershfield, and Christopher Stanton

Physics Department, University of Florida

Jian Chen

Seagate Technology

(15 March, 2000)

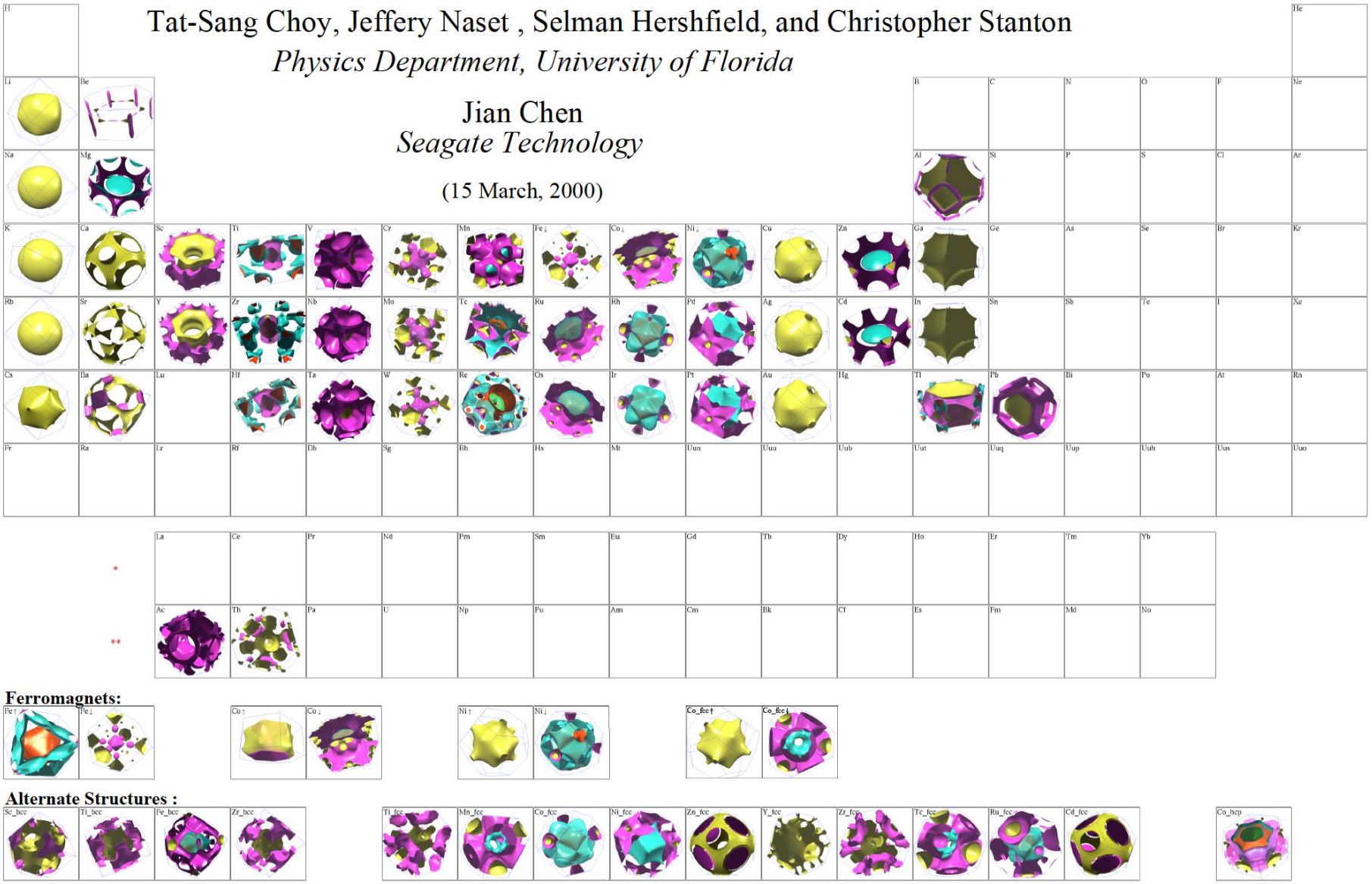

Ferromagnets:

Alternate Structures :

Source of tight binding parameters (except for fcc Co ferromagnet): D.A. Papaconstantopoulos, *Handbook of the band structure of elemental solids*, Plenum 1986.

This work is supported by NSF, AFOSR, Research Corporation, and a Sun Microsystems Academic Equipment Grant.

Band mapping

- Angle-resolved photoemission spectroscopy (ARPES)

$$E_k = h\nu - \Phi - E_B$$

work function　　binding energy

$$k_{||}(\text{Å}^{-1}) = 0.512\ \{(h\nu-\Phi-E_B)\}^{1/2} \cdot \sin\theta_e$$

$$k_{z,in} = \sqrt{k_{z,out}^2 + (0.512)^2 V_0}$$

Vo: inner potential

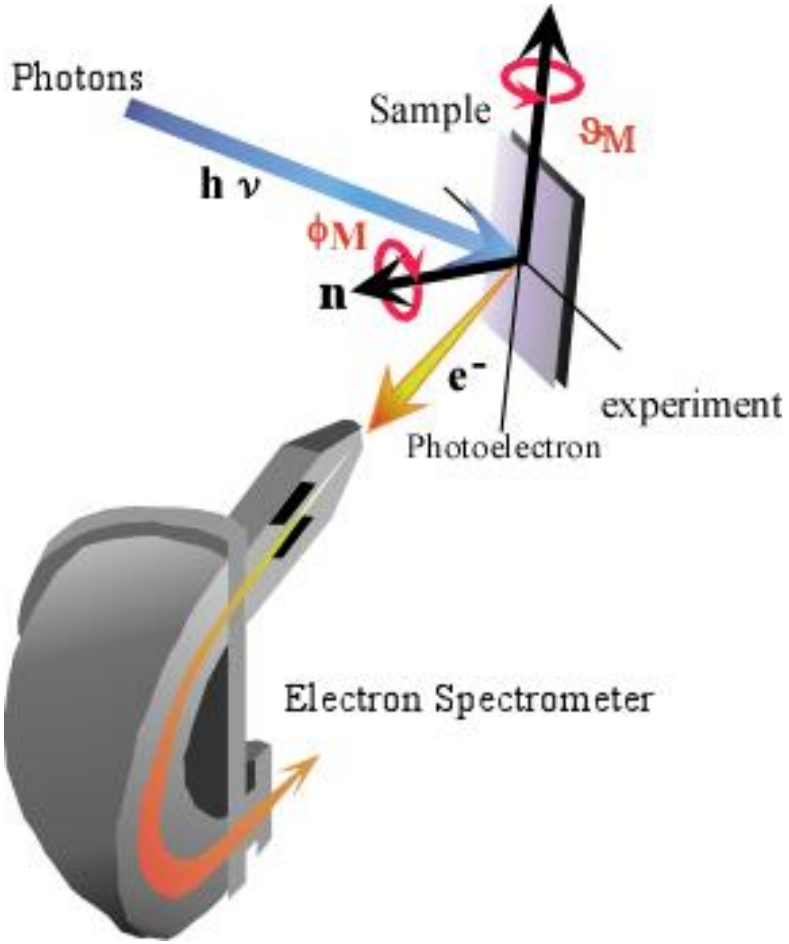

→ Band dispersion（E,k）

→ Fermi surface（E_F,k_F）

Exp. Setups

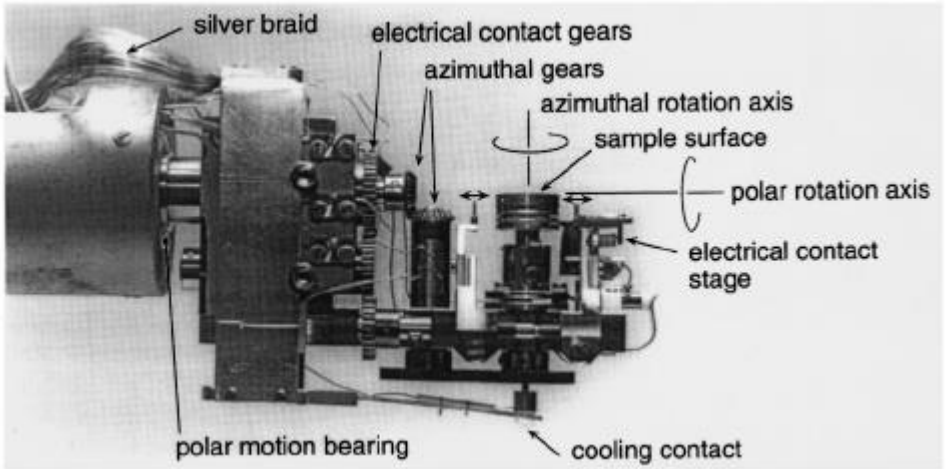
silver braid
electrical contact gears
azimuthal gears
azimuthal rotation axis
sample surface
polar rotation axis
electrical contact stage
polar motion bearing
cooling contact

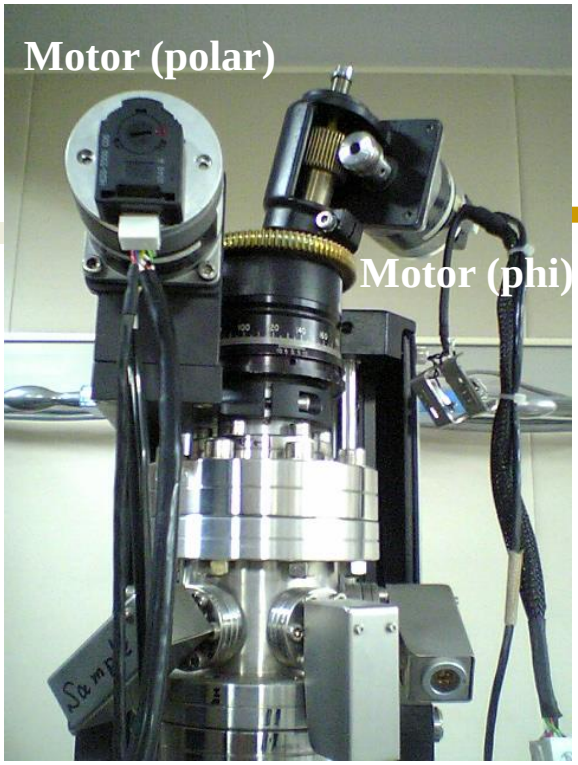
Motor (polar)
Motor (phi)

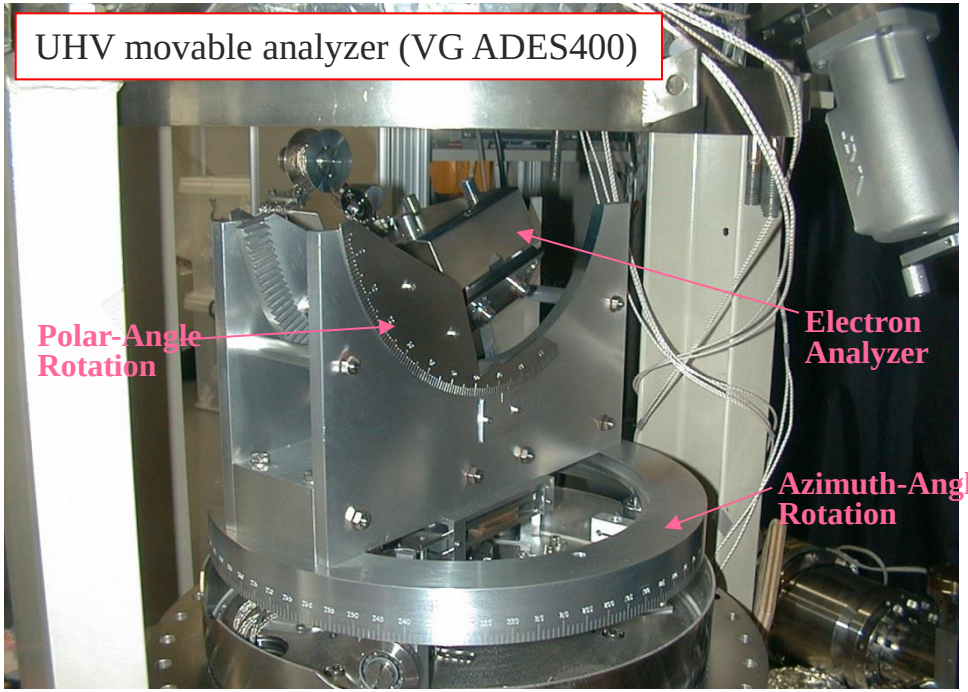
UHV movable analyzer (VG ADES400)
Polar-Angle Rotation
Electron Analyzer
Azimuth-Angle Rotation

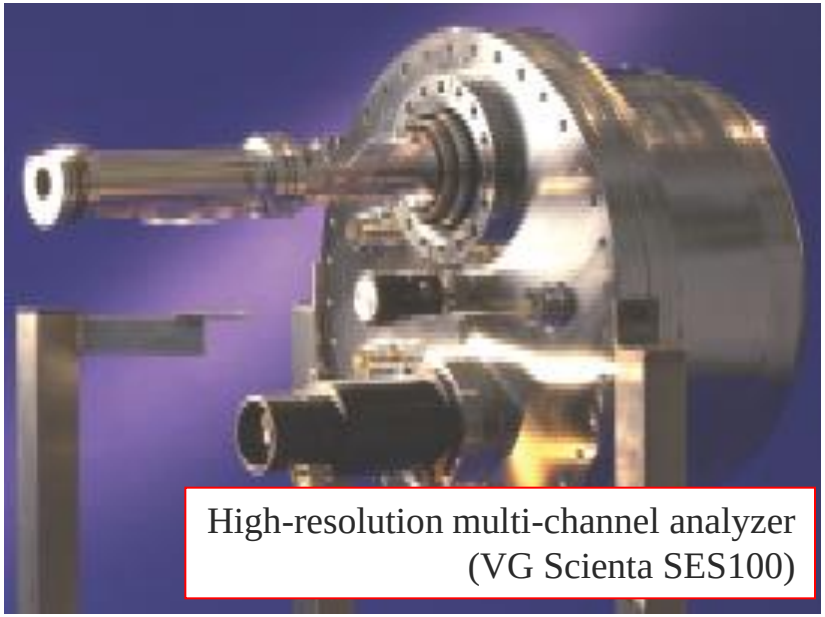
High-resolution multi-channel analyzer (VG Scienta SES100)

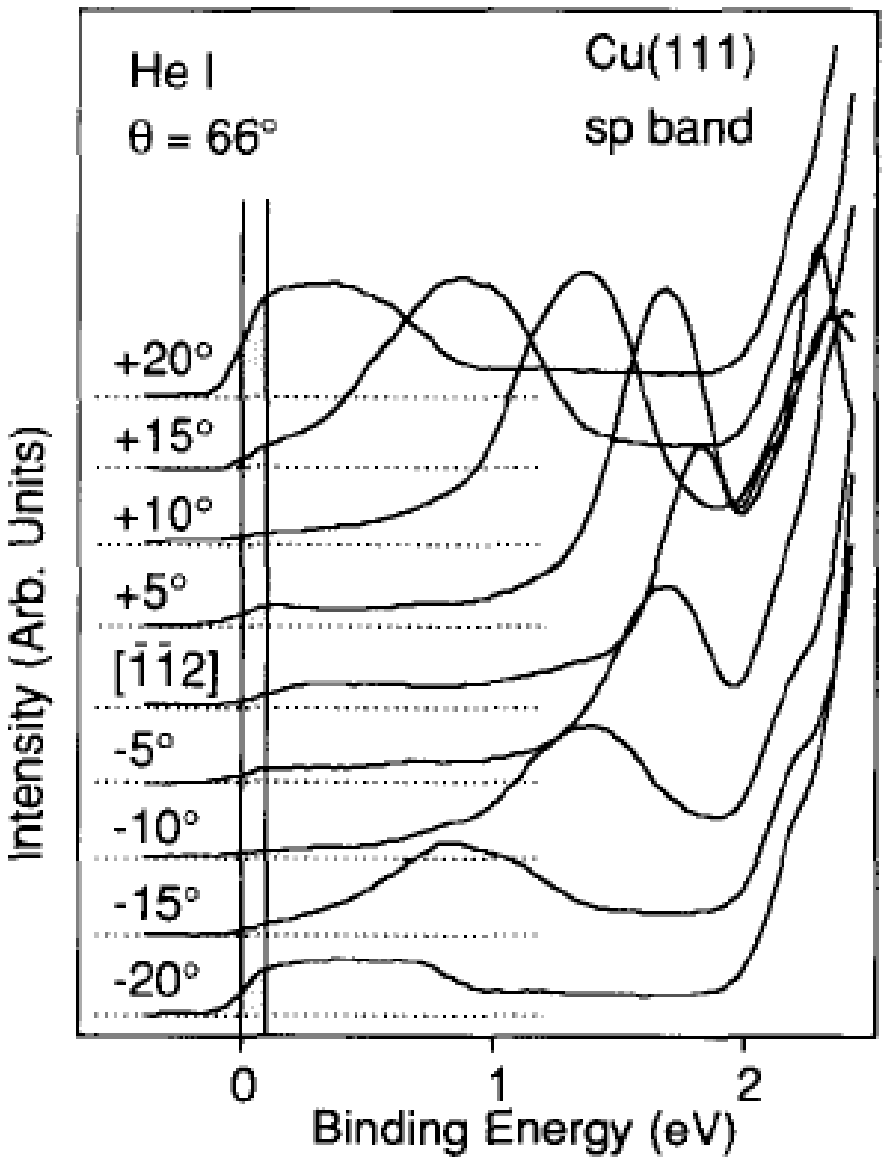

Cu(001)

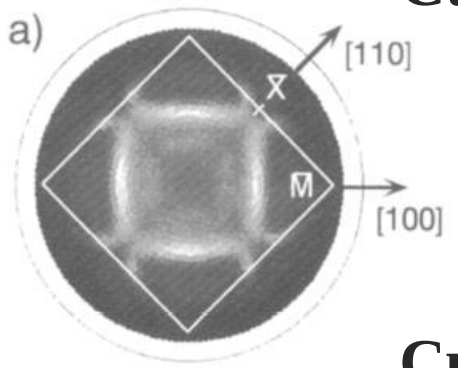

Cu(111)

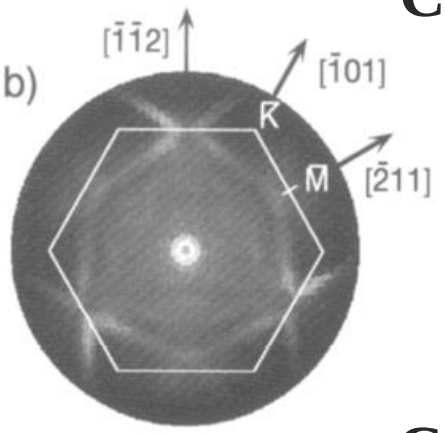

Cu(110)

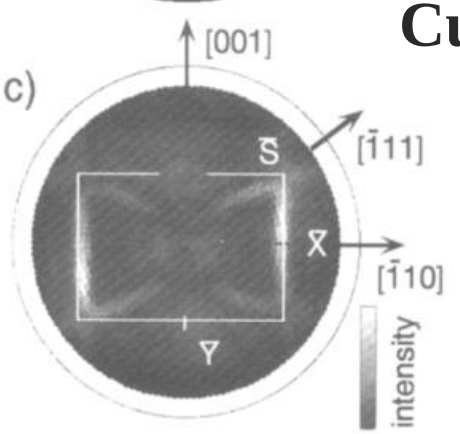

P. Aebi *et al.*, Surf. Sci. **307-309**, 917 (1994).

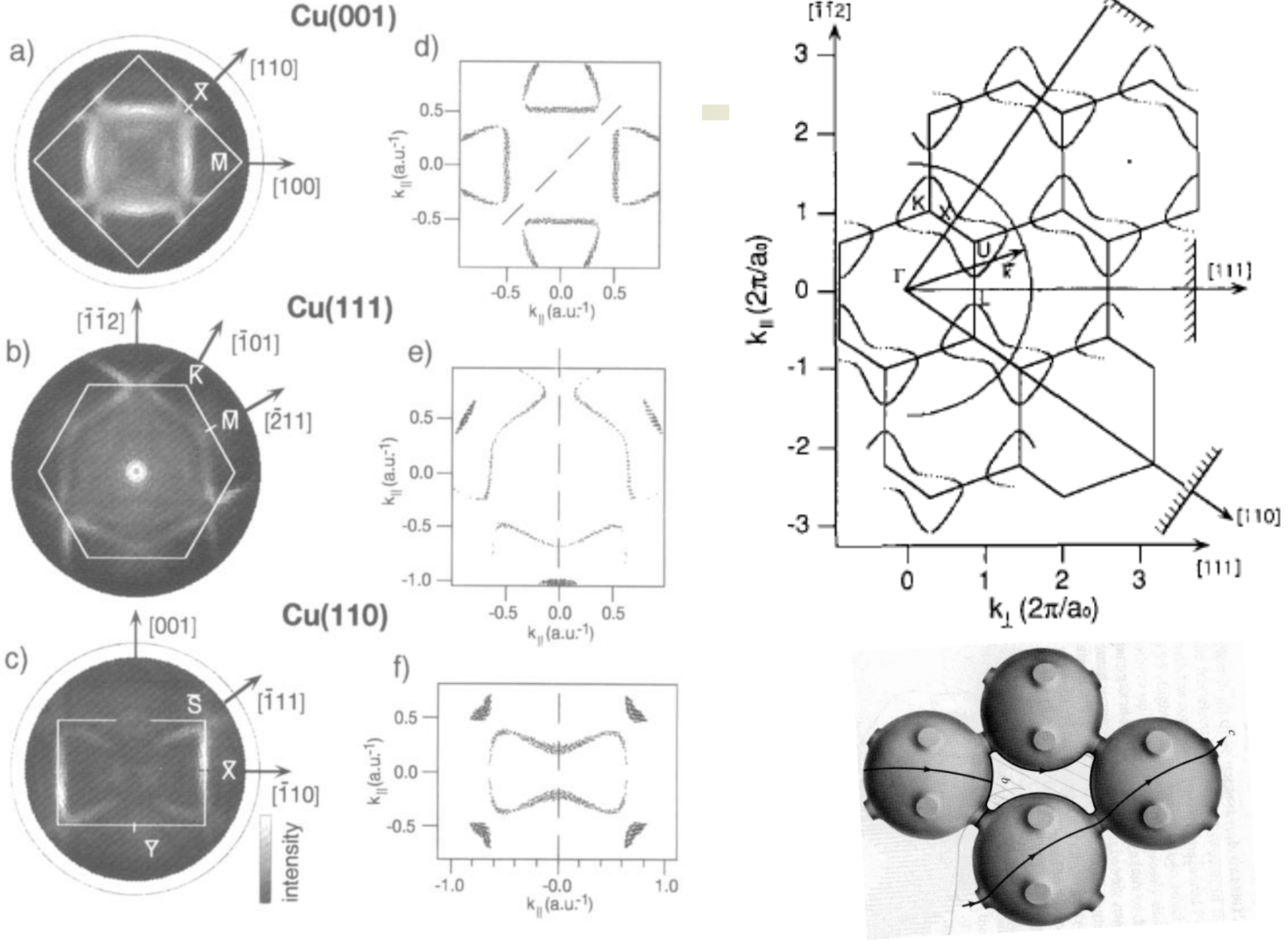
Cu(001)
a)
[110]
[100]
X
M
d)
0.5
0.0
-0.5
$k_{||}$ (a.u.$^{-1}$)
Cu(111)
b)
[$\bar{1}\bar{1}$2]
[$\bar{1}$01]
[$\bar{2}$11]
K
M
e)
Cu(110)
c)
[001]
[$\bar{1}$11]
[$\bar{1}$10]
S
X
Y
intensity
f)
-1.0
1.0
[001]
[$\bar{1}\bar{1}$2]
[111]
[110]
$k_{||}$ ($2\pi/a_0$)
$k_{\perp}$ ($2\pi/a_0$)
Γ
K
X
U

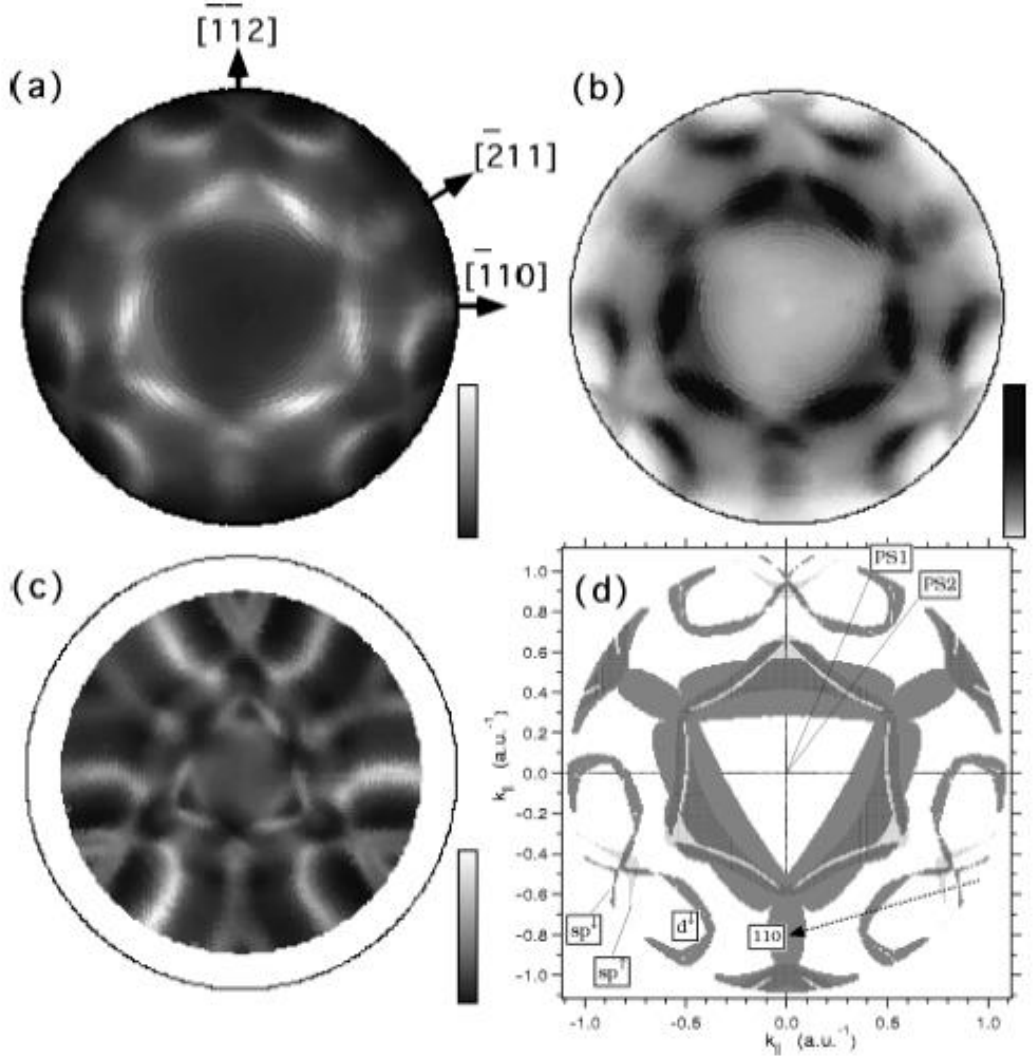

FIG. 3. He I-excited Fermi-surface map from Ni(111). In (a) and (b) the raw data are presented in parallel projection. In (a), high intensities are shown in white, while in (b) the grey scale is inverted with slightly enhanced contrast. (c) shows the data in stereographic projection and normalized with "ϕ average" (see Sec. II B). In (d) the corresponding LKKR calculation is displayed. "PS1" and "PS2" indicate the direction of the angle-scanned EDCs from Sec. III C, Figs. 9 and 10, respectively. The dashed arrow tagged "110" roughly follows the line in **k** space corresponding to the polar scan on Ni(110) discussed in Ref. 34.

T. J. Kreutz *et al.*, Phys. Rev. B **58**, 1300 (1998).

Ni(111)

T_C=631 K

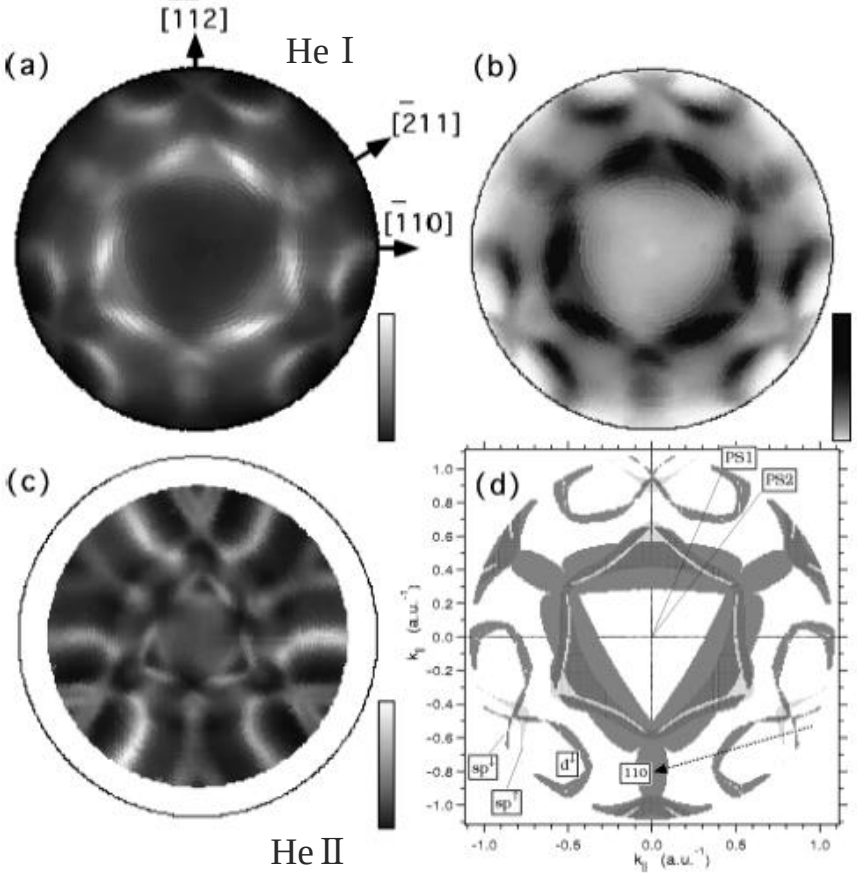

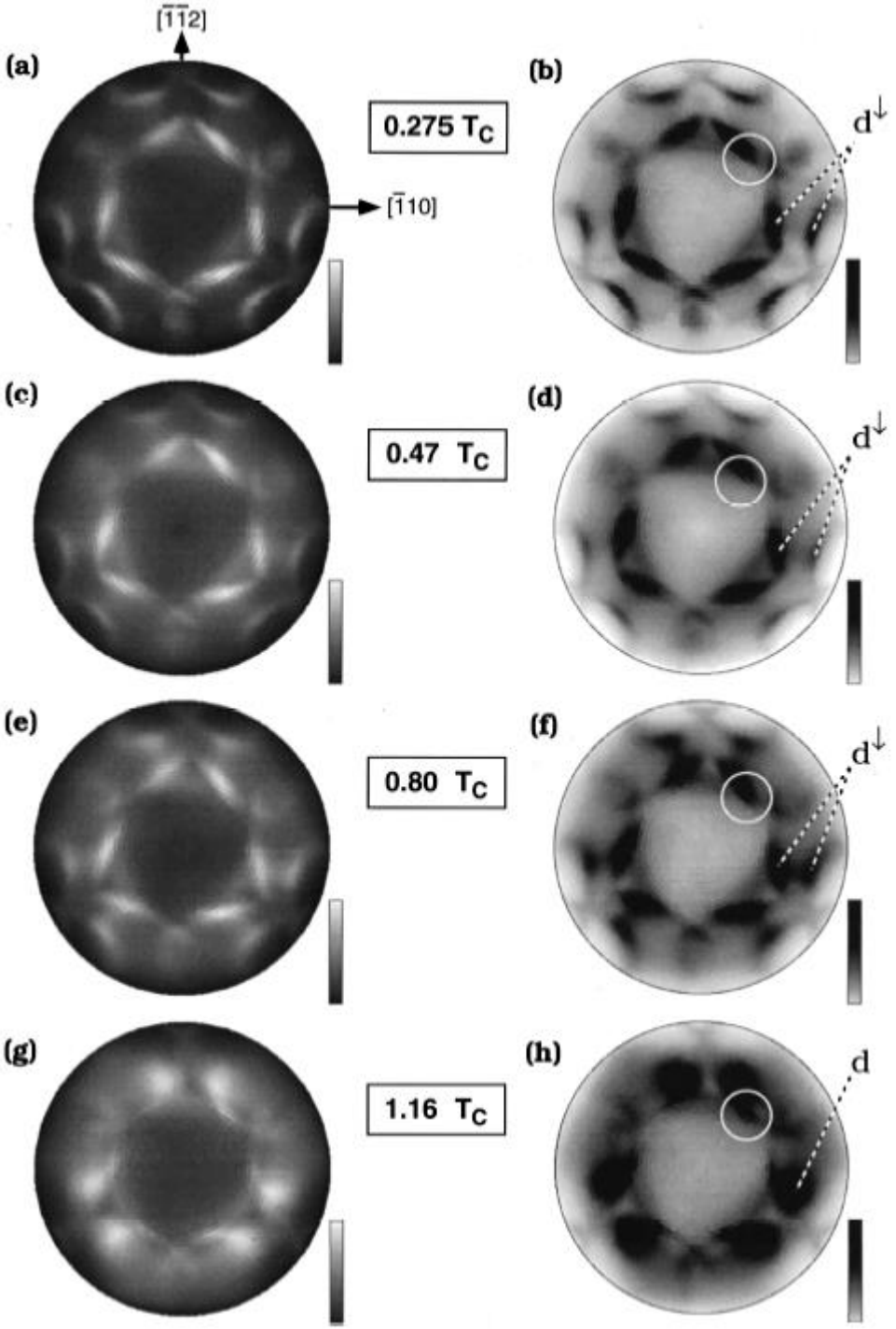

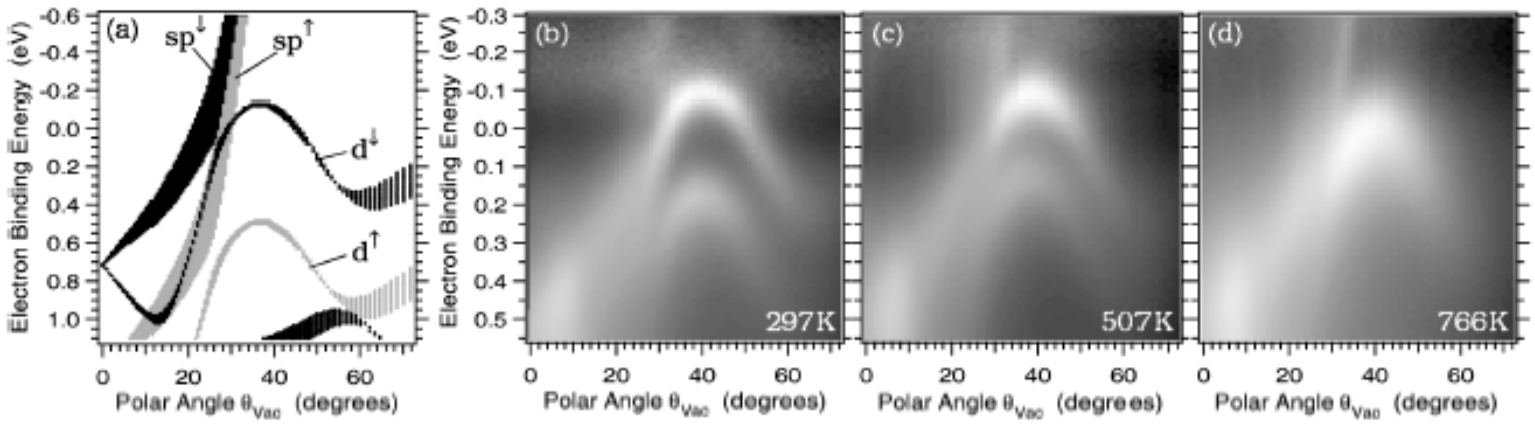

FIG. 3. (a) Spin-polarized LKKR calculation covering the section in $\vec{k}$ space of our measurements. Majority spin bands are given in gray, minority bands in black. (b)–(d): He $I\alpha$ excited polar-angle scanned EDCs taken from Ni(111) along the azimuth which is 67° off the $[\bar{1}10]$ direction and 23° off $[\bar{1}\bar{1}2]$, measured at three different temperatures: (b) $0.47T_c$, (c) $0.80T_c$, and (d) $1.21T_c$. All spectra have been normalized by a Fermi-Dirac distribution function which rides on a small constant background in order to avoid zero divisions. The linear gray scale ranges from minimum (black) to maximum (white) intensity.

Ni Ferromagnetic transition

→ Stoner-type

T. Greber *et al.*, Phys. Rev. Lett. **79**, 4465 (1997).

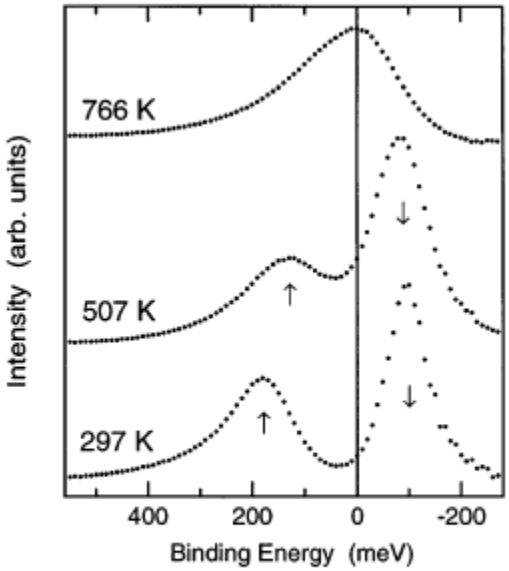

FIG. 4. EDCs extracted from the normalized data of Fig. 3(b)–3(d) at the apex of the d bands ($\theta = 40°$). Spin labels are indicated by the arrows. The curves are drawn with intensity offsets.

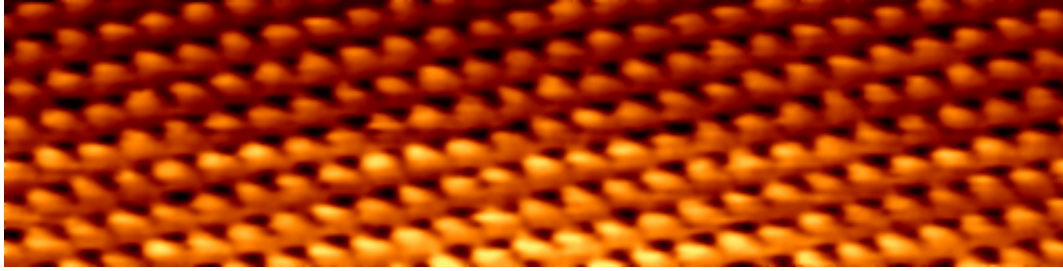

Cu(111)

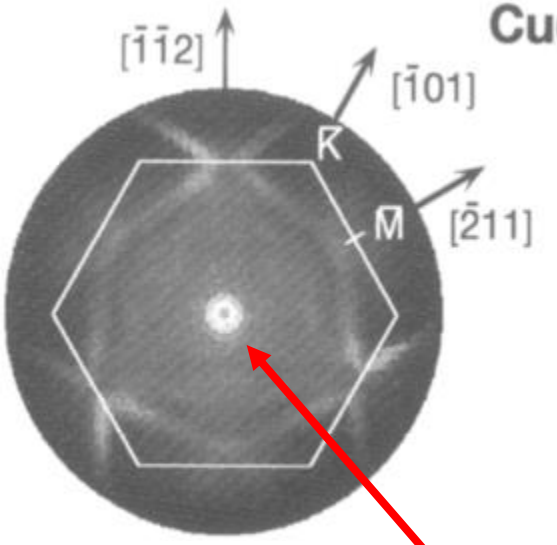

Surface state in L point gap

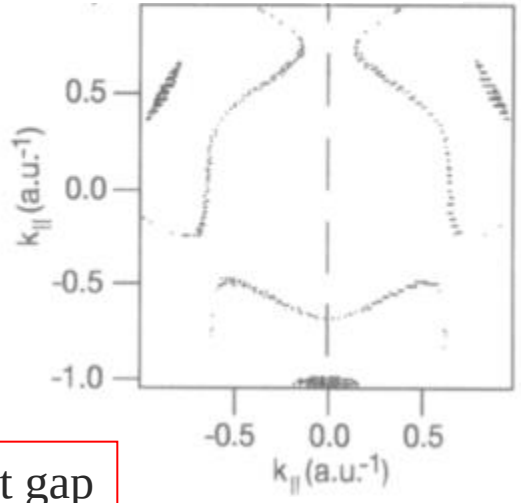

L点 gap

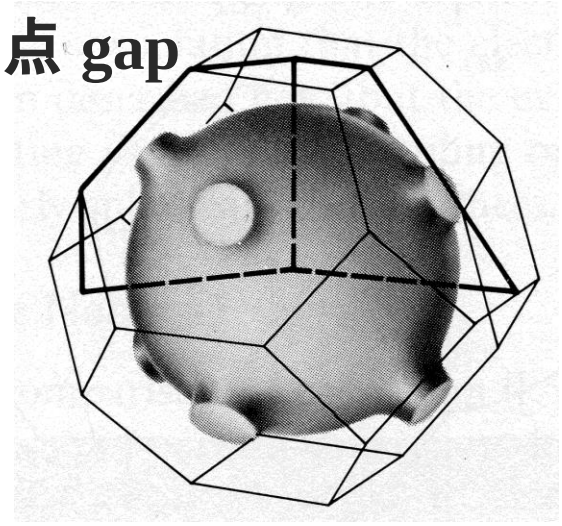

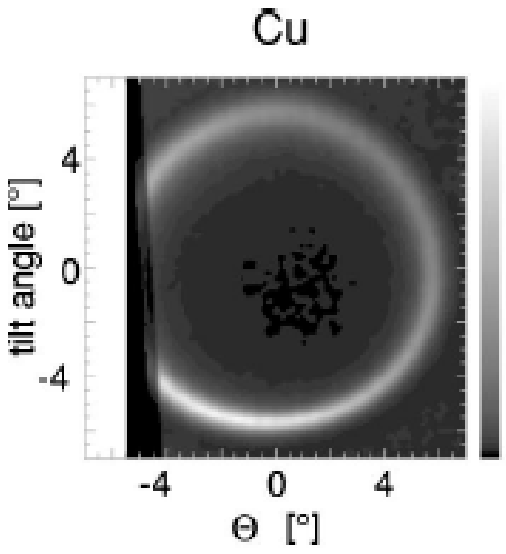

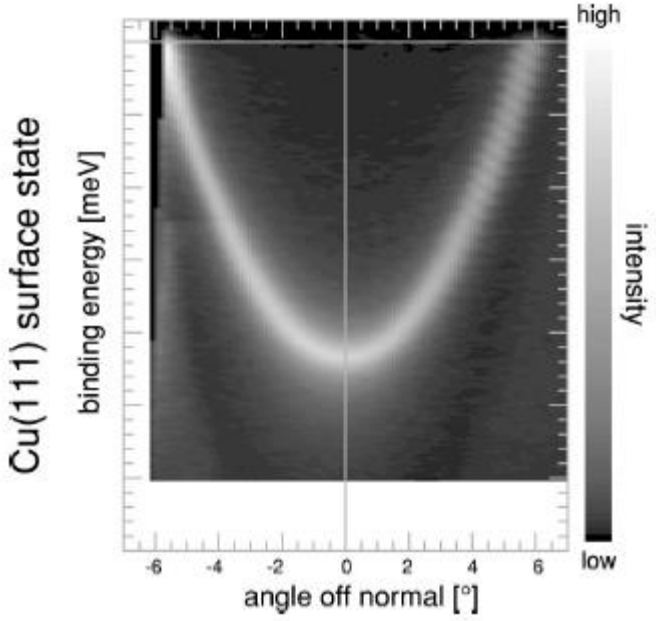

F. Reinert *et al.*,
Phys. Rev. B **63**, 115415 (2001).

Ag(111)

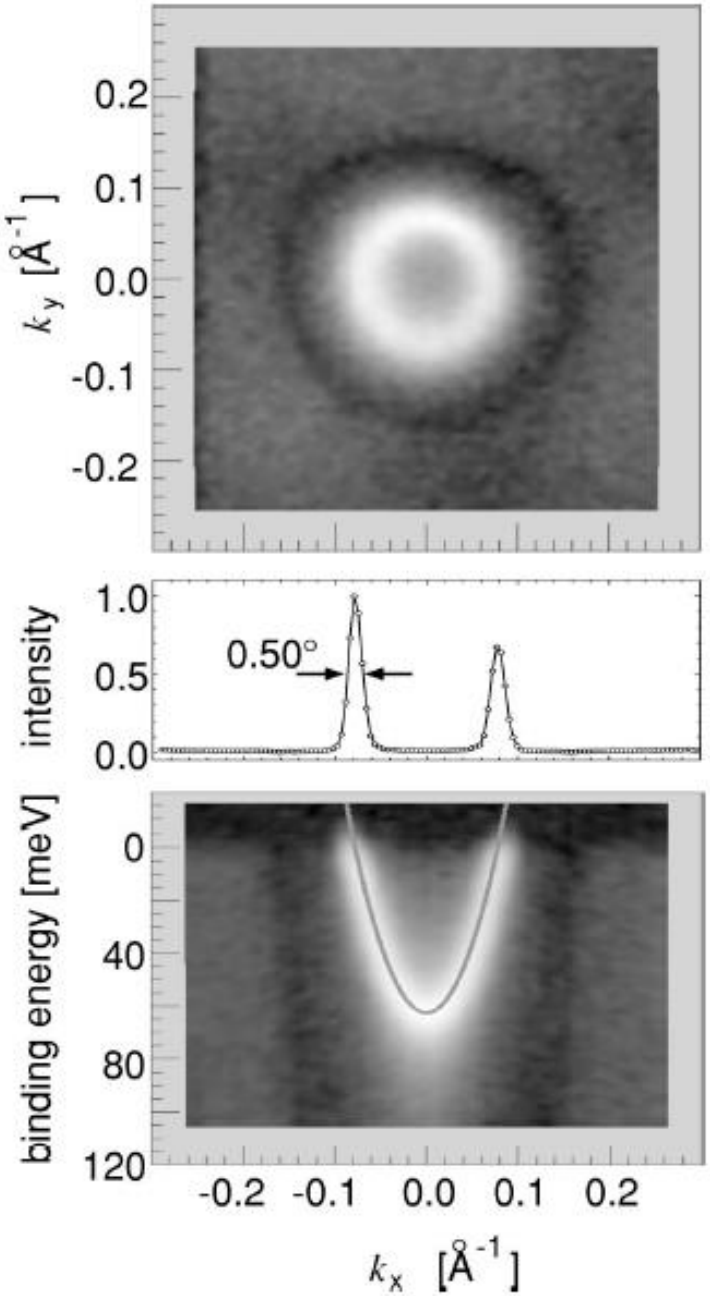

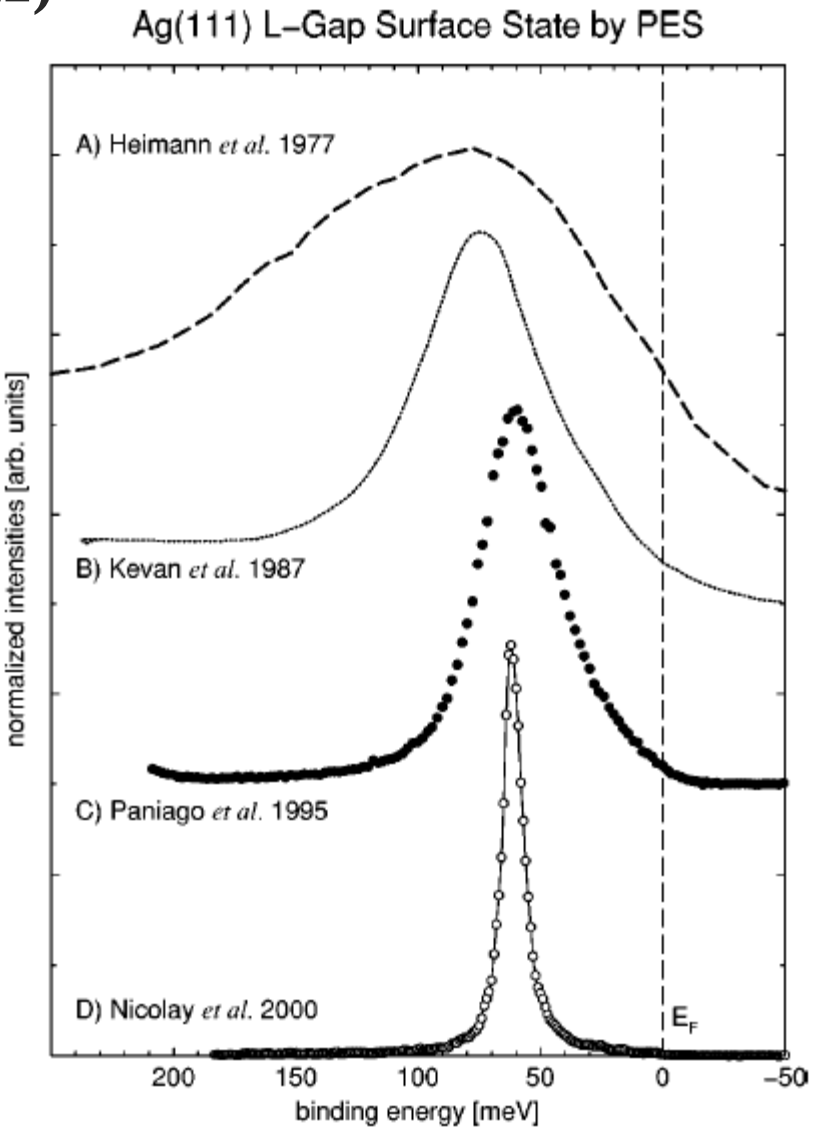

F. Reinert *et al.*, Phys. Rev. B **63**, 115415 (2001).

G. Nicolay *et al.*, Phys. Rev. B **65**, 033407 (2001).

Au(111)

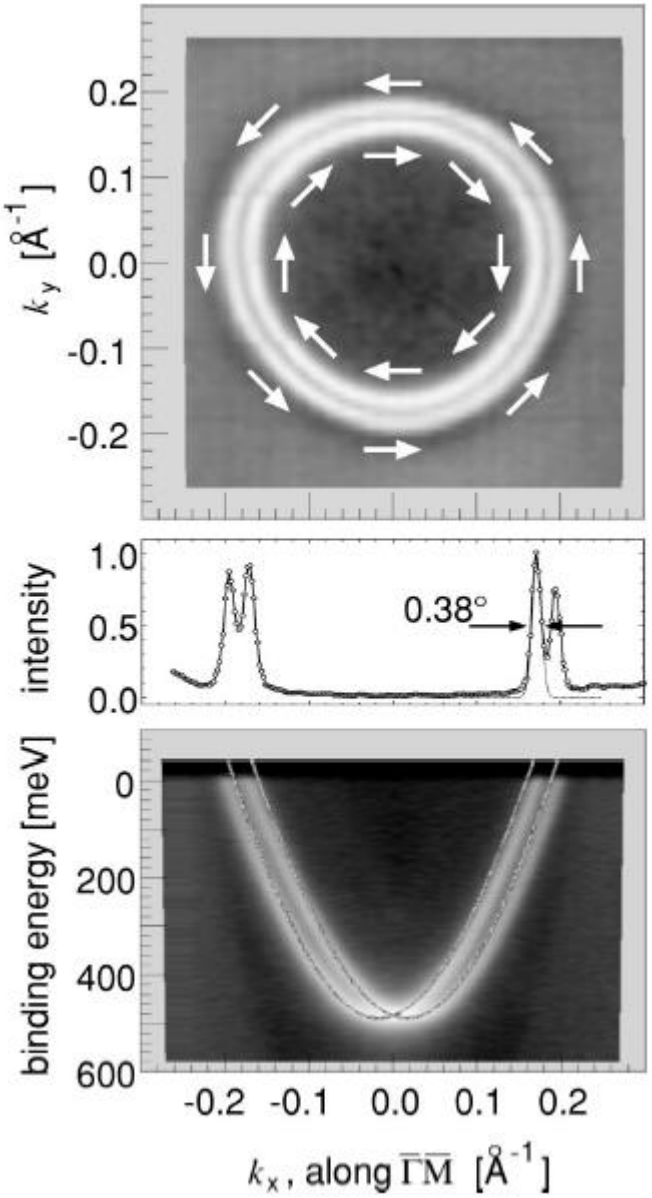

Spin-orbit splitting

$$H_{SOC} = \frac{\mu_B}{2c^2}(\mathbf{v} \times \boldsymbol{\mathcal{E}}) \cdot \boldsymbol{\sigma},$$

$$E^{\uparrow,\downarrow}(k) = E_0 + \frac{\hbar^2 k^2}{2m^*} \pm \alpha k = E_0' + \frac{\hbar^2 (k \pm k_0)^2}{2m^*},$$

↓

Spin-slit surface-state band

↓

Spin-resolved photoemission spectroscopy

J. Henk *et al.*, Phys. Rev. B **68**, 165416 (2003)

Fermi surface mapping with spin-resolved photoemission spectroscopy

H. Moritz *et al.*, J. Elec. Spec. Rel. Phenom. **124**, 263 (2002).

kx,ky,kz,σx,σy,σz are determined with synchrotron radiation

COmplete PHotoEmission Experiment (COPHEE)

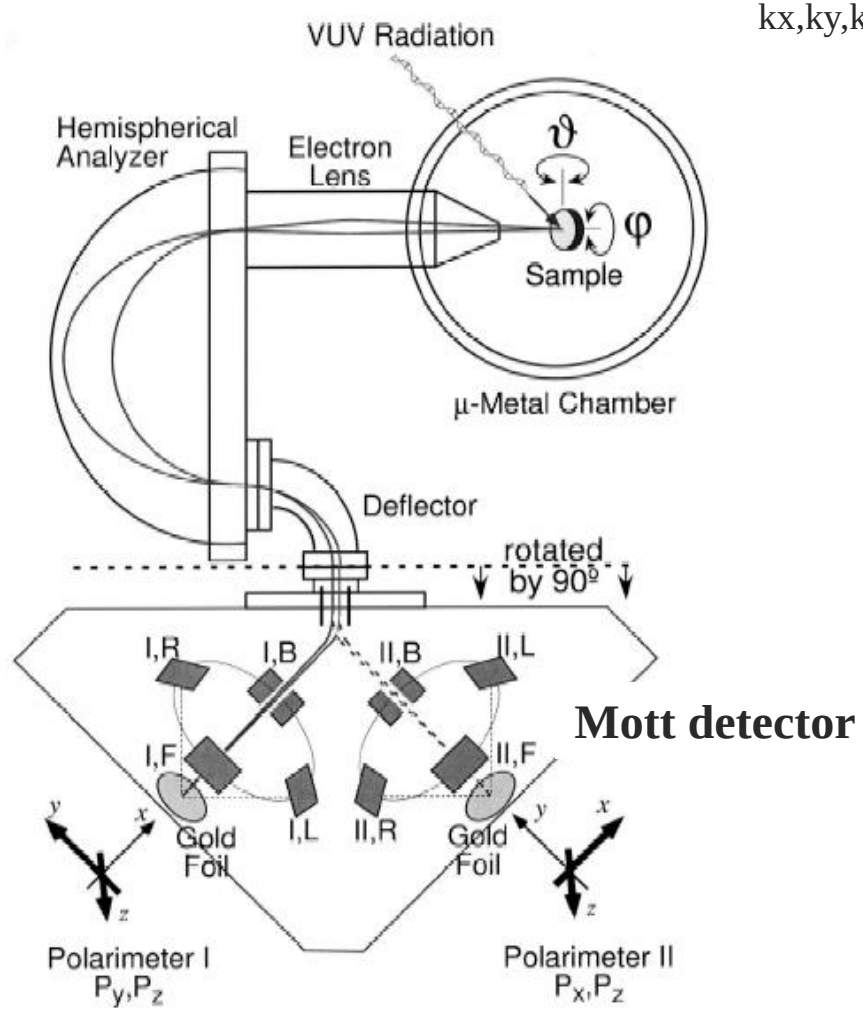

Mott detector

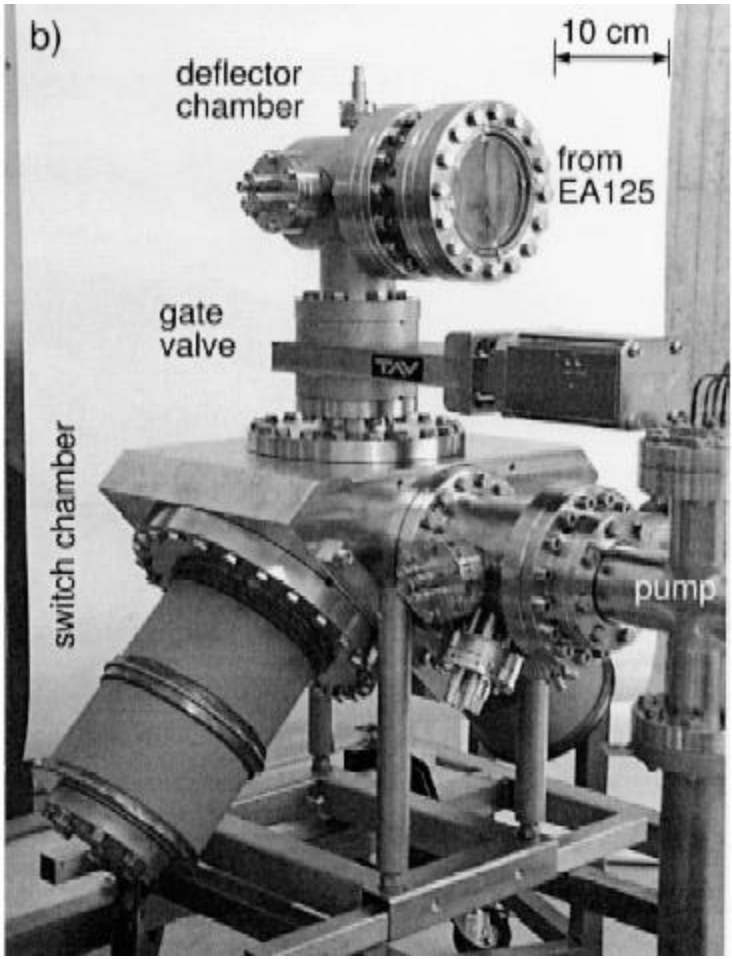

Fig. 4. Schematic view of COPHEE, the COmplete PHotoEmission Experiment. Electrons photoemitted from a sample by UV radiation are energy- and angle-selected by an electrostatic analyzer and detected in two orthogonal Mott polarimeters. In an electrostatic beam deflection system the spin direction is conserved and polarimeter I measures the polarization components P_y and P_z, while polarimeter II measures P_x and P_z. The beam is switched between the two to allow quasi-simultaneous data collection. The labels of the detectors are used in Eq. (10) in the text. The polarimeter system is shown rotated by 90° for graphical clarity.

Au(111)

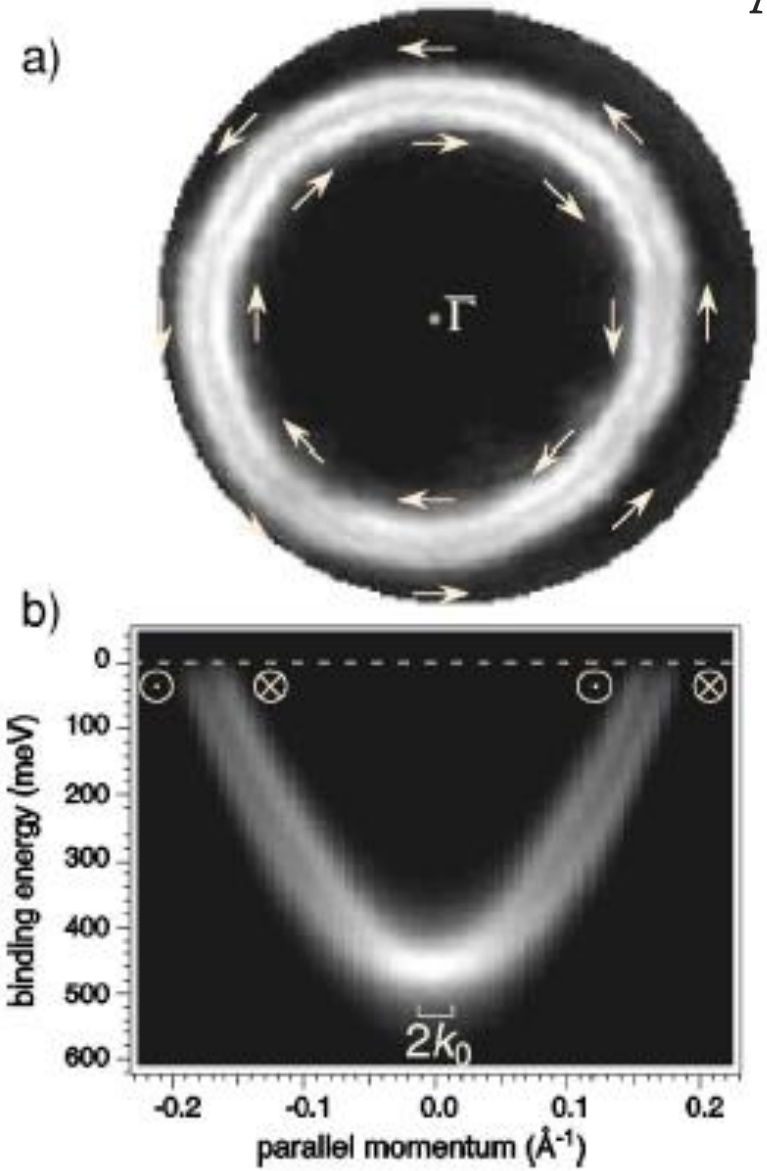

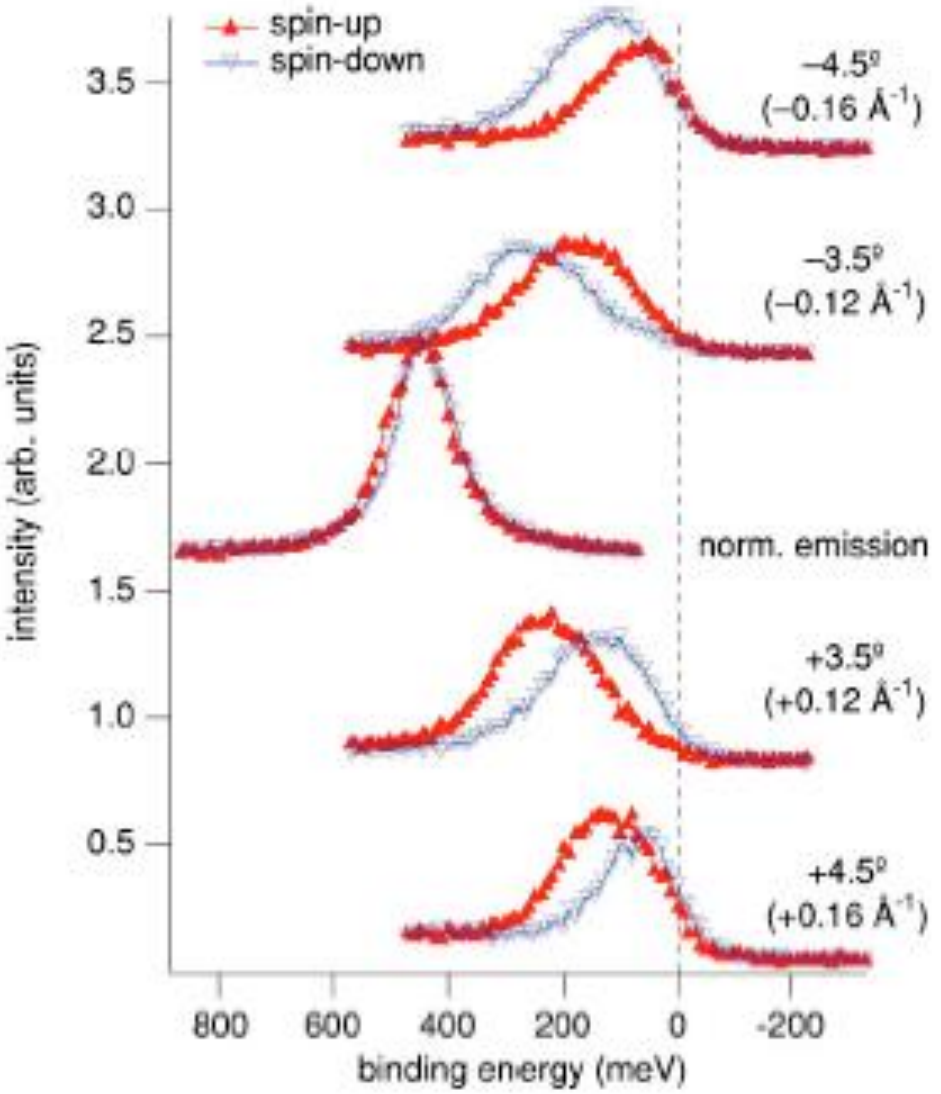

M. Hoesch *et al*., Phys. Rev. B **69**, 241401(R) (2004)

Au(111)

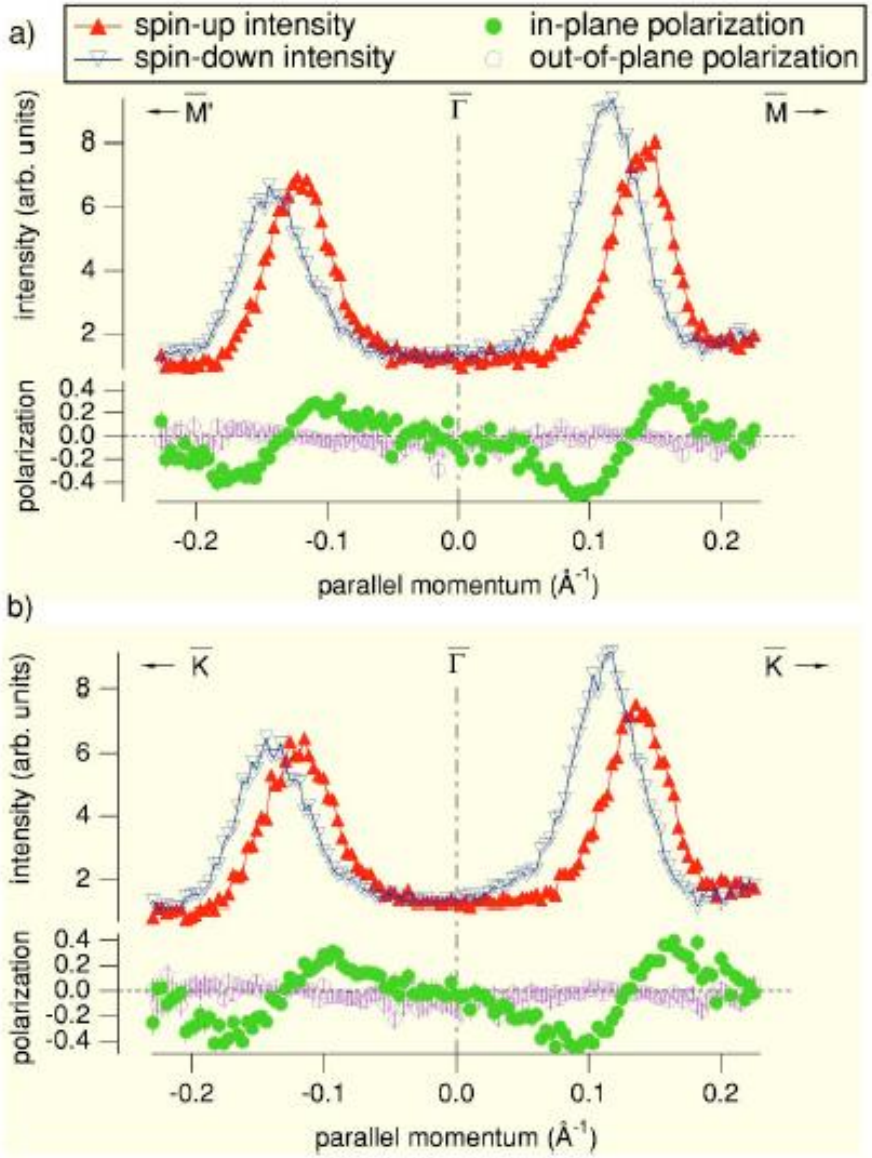
a)
spin-up intensity
spin-down intensity
in-plane polarization
out-of-plane polarization
M'
Γ
M
intensity (arb. units)
polarization
parallel momentum (Å^{-1})
b)
K
Γ
K
intensity (arb. units)
polarization
parallel momentum (Å^{-1})

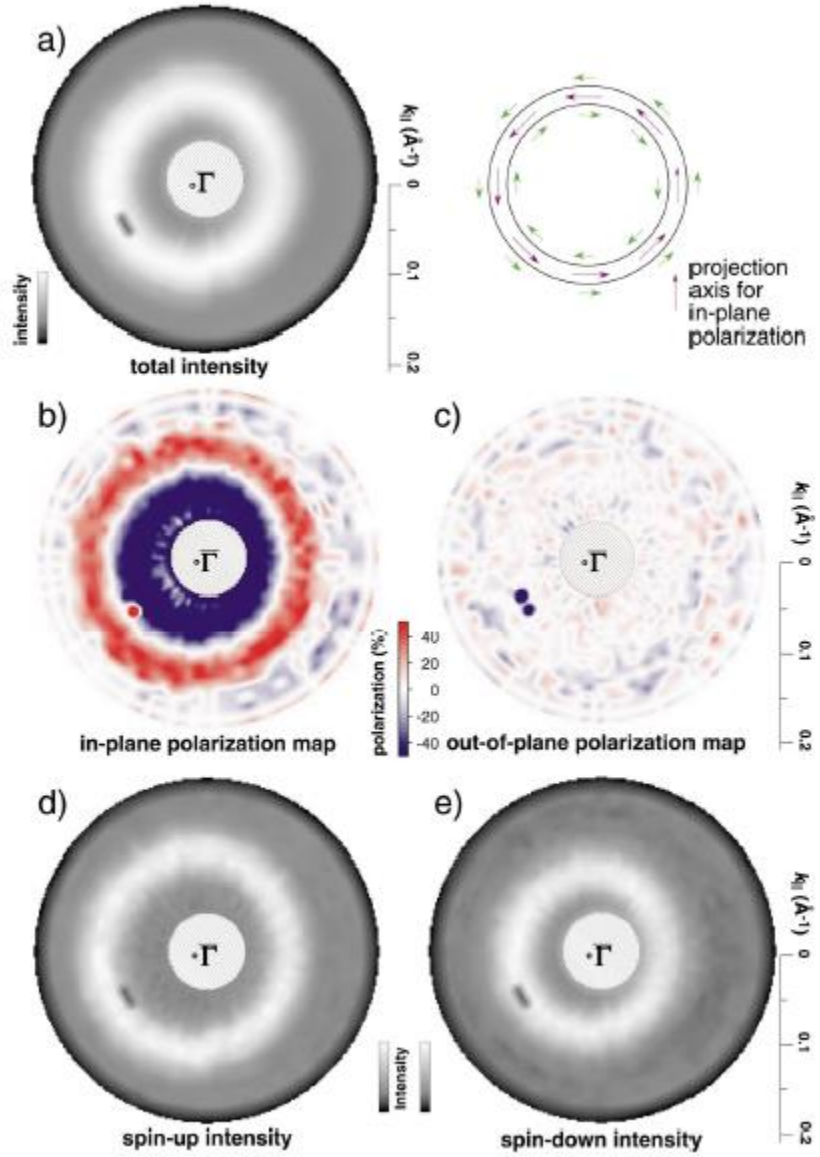
a)
total intensity
projection axis for in-plane polarization
b)
in-plane polarization map
c)
out-of-plane polarization map
polarization (%)
d)
spin-up intensity
e)
spin-down intensity
intensity
$k_{||}$ (Å^{-1})

Modern photoemission techniques

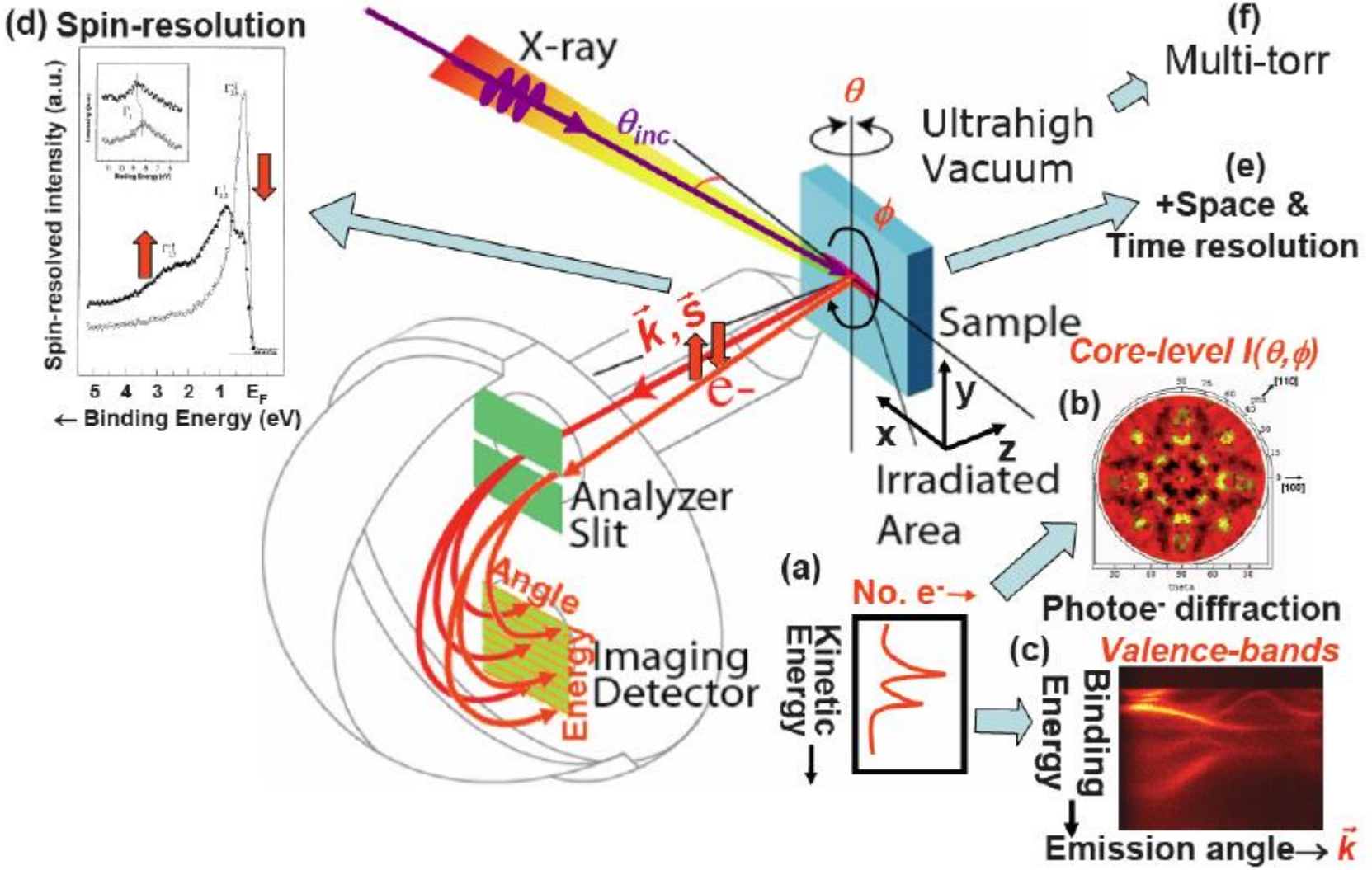

C.S. Fadley

Frontier Spectroscopy experiments at SPring-8 BL07LSU:

with time-resolution and at nano-space

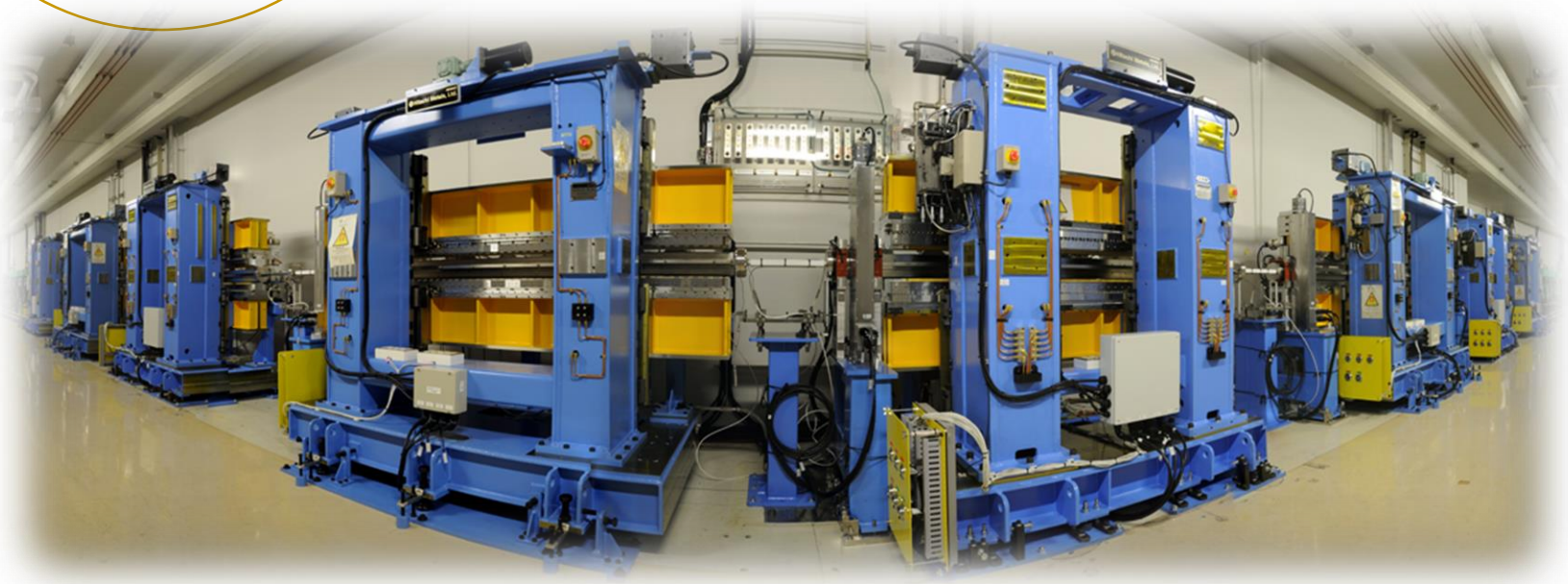

SPring-8 BL07LSU

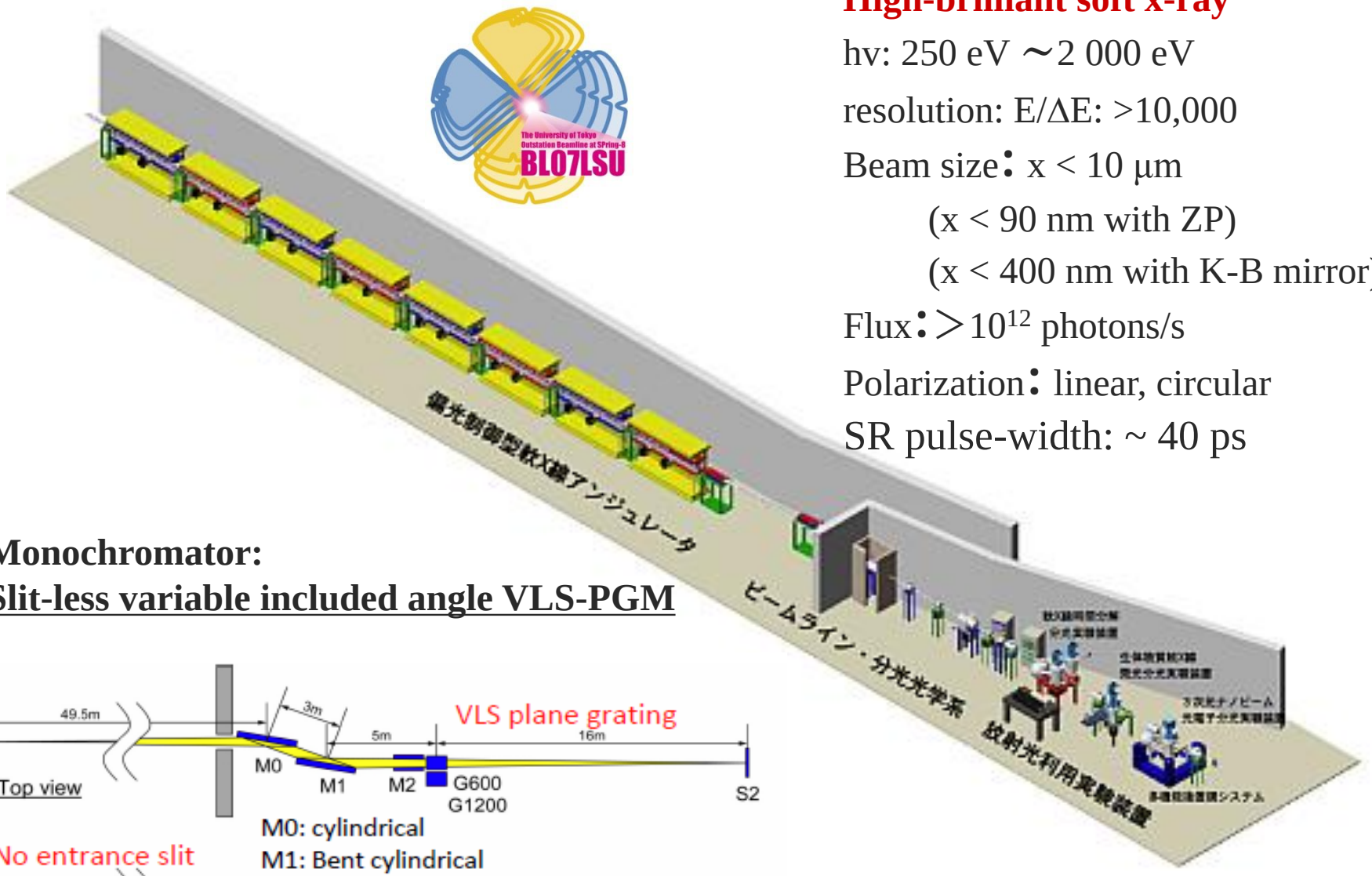

Specification

High-brilliant soft x-ray

hv: 250 eV ～2 000 eV

resolution: E/ΔE: >10,000

Beam size: x < 10 μm

(x < 90 nm with ZP)

(x < 400 nm with K-B mirror)

Flux: $> 10^{12}$ photons/s

Polarization: linear, circular

SR pulse-width: ~ 40 ps

Monochromator:

Slit-less variable included angle VLS-PGM

3D-scanning photoelectron microscope

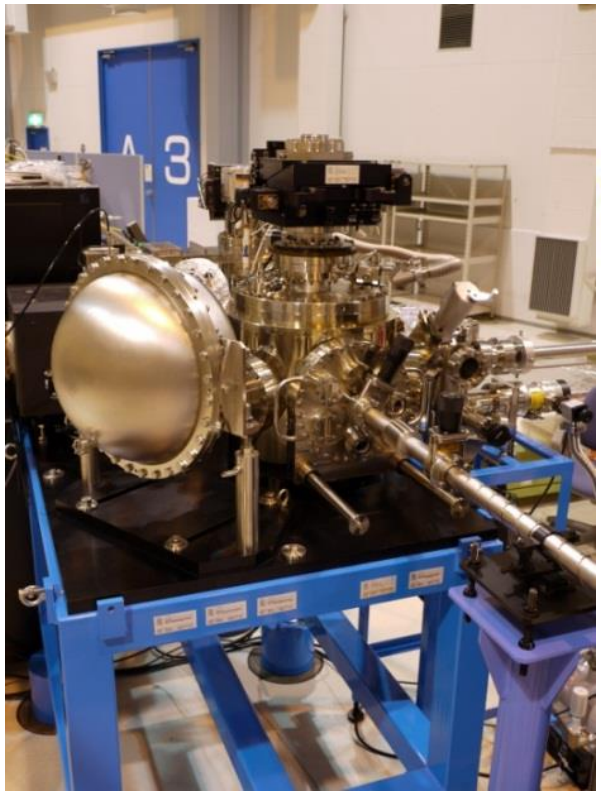

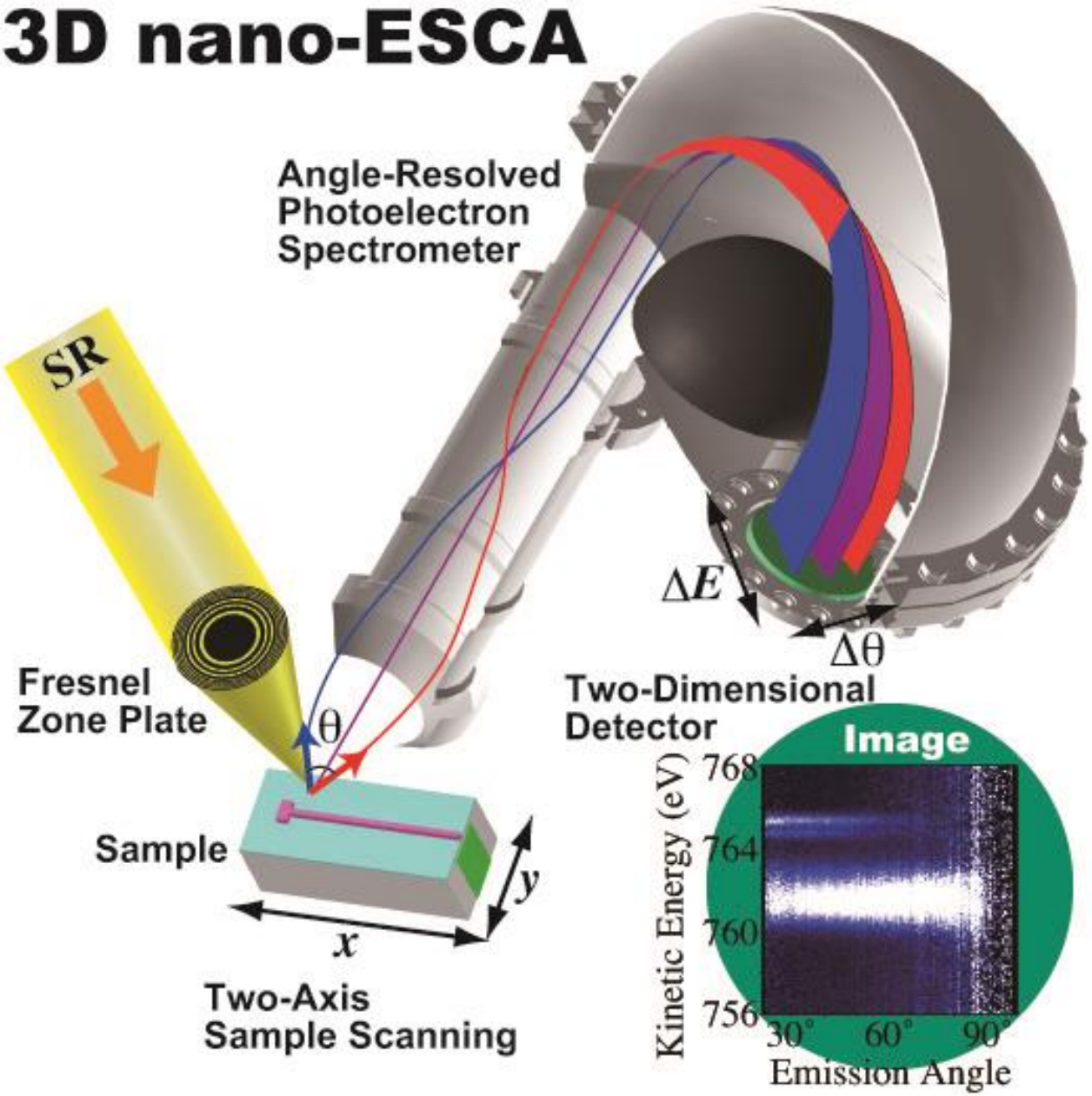

雰囲気光電子分光

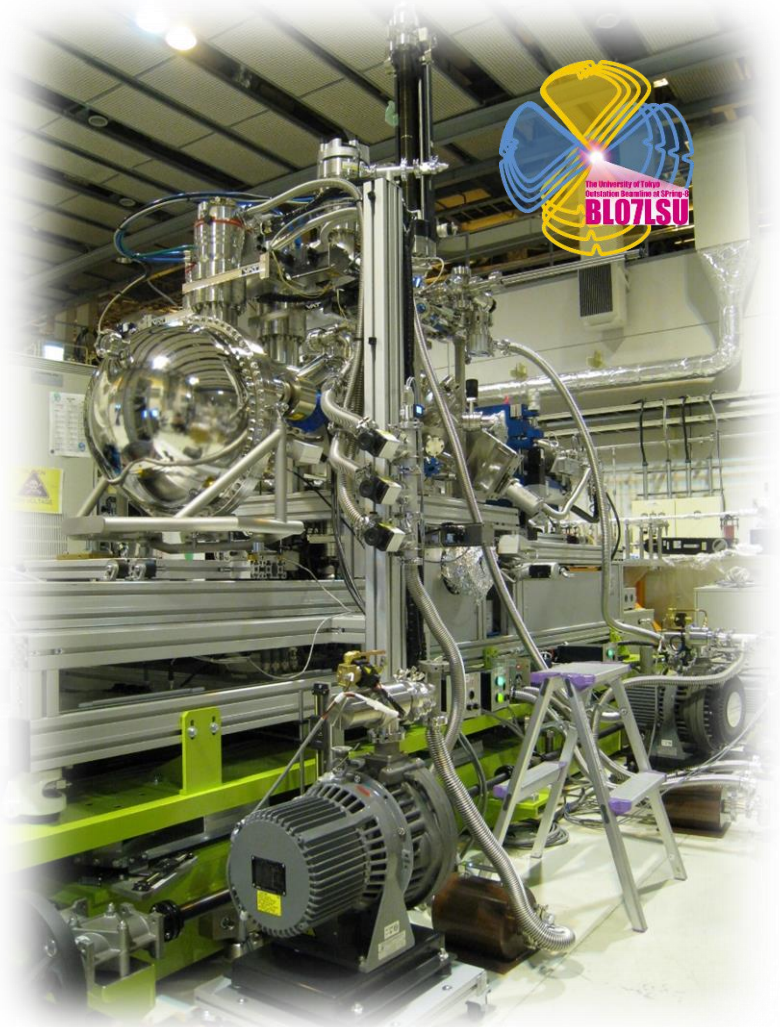

雰囲気光電子分光システム
@SPring-8 BL07LSU

「雰囲気光電子分光システム」
世界最高レベルの気体雰囲気中での
光電子分光測定を実現

- 超高輝度放射光　SPring-8 BL07LSU
  フリーポートステーション
- 差動排気型電子分光器
- 小体積ガスセル
  →up to 20 mbar（世界最高レベル）

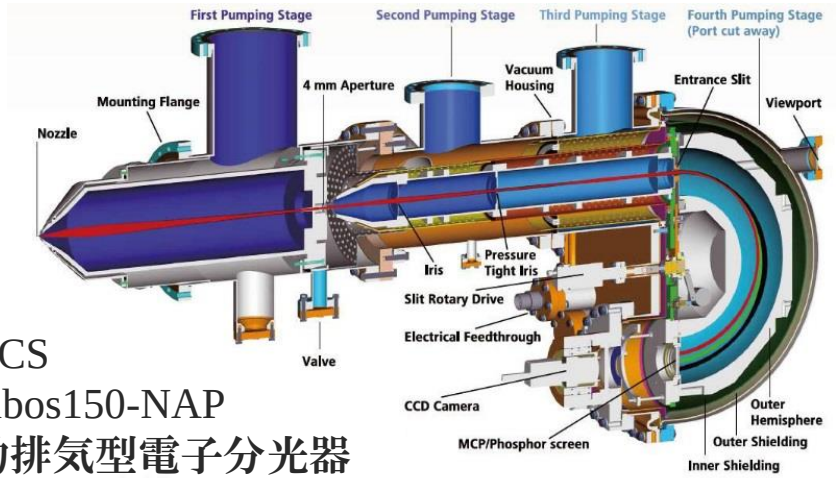

SPECS
Phoibos150-NAP
差動排気型電子分光器

The future in photoemission spectroscopy (Vol. 27, No. 2, 2014, Synchrotron radiation news)

SRN
Synchrotron Radiation News
ISSN 0894-0886 is published bi-monthly.
Coden Code: SRN EFR

Heather Wagner, *Content Director*
Maureen Williams, *Advertising Manager*
Patrick Hufnagle, *Designer*

Editorial Services
Synchrotron Radiation News
1231 Hawk Ridge Road
Lafayette, CO 80026, USA
E-mail: HLWagner@comcast.net

Advertising Services
Maureen Williams
PO Box 449
Point Pleasant, PA 18950, USA
E-mail: mwilliams@cisaz.com

Circulation and Subscriptions
Taylor & Francis Group, LLC
530 Walnut Street, Ste. 850
Philadelphia, PA 19106, USA
Tel: + 1 215 625 8900
Fax: + 1 215 207 0050

The following subscriptions are available:
Vol. 27 (2014), six issues.
Individual, print only:
$173/£104/€136
Institutional, print+online:
$1,278/£774/€1,020
Institutional, online only:
$1,118/£677/€893

http://tandfonline.com/toc/gsrn20/current

The Future of Photoemission Spectroscopy

This issue of *SRN* focuses on photoelectron spectroscopy, a technique that is flourishing at many synchrotron facilities worldwide. In a nutshell, it is a simple technique making use of the photoelectric effect and benefiting from the bright light available at synchrotrons. In the past two decades, one of its branches, angle-resolved photoemission (ARPES), has gained tremendous popularity due to its ability to provide insights into the physics of strongly correlated materials such as, for example, the high Tc superconductors. Its success rests on advances in instrumentation which, over the course of many years, have led to dramatic improvements in resolution in both energy and momentum.

In this issue, we wish to bring attention to four rapidly developing subfields: photoemission, with the ability to resolve the spin of the photoelectrons; ambient pressure photoemission which tracks chemical reactions at the surfaces; nano-ARPES, a technique enabled by the advances in our ability to focus soft X-rays into a small spot on the sample; and ARPES utilizing soft X-rays for enhanced bulk sensitivity. Some of these techniques are not exactly new kids on the block. Spin-resolved photoemission can be traced back to a 1969 paper by G. Busch et al. [1]. Ambient pressure photoemission probably started with the invention of a "high-pressure" electron spectrometer by R. Joyner et al. [2]. Nano-ARPES has emerged from the early efforts to use Schwarzschild optics or zone plates for collecting photoemission spectra, mostly for chemical analysis, with a good lateral resolution [3]. Unlike regular ARPES, however, despite being "old" techniques, they have been actively practiced in just a handful of places.

A renaissance of interest in spin-resolved photoemission has come about with the discovery of topological insulators with surface electronic states possessing peculiar spin textures. Spin-resolved ARPES seems to be the only technique capable of probing these states in the most direct way. As new proposals are being put forward to use materials with all sorts of unusual spin textures in spintronics devices (e.g., as spin generators, etc.), demand for spin-resolved photoemission measurements keeps growing. The report by N. Mannella of the University of Tennessee at Knoxville reviews the origins of spin-polarization in photoemission. His article is a timely reminder that the spin polarization of photoelectrons is not necessarily a direct reflection of the spin textures existing within the material, and numerous factors leading to the polarization of photoemitted electrons must be considered while analyzing the data.

The article by A. Shavorskiy, O. Karslioglu, I. Zegkinoglou, and H. Bluhm, a team practicing ambient pressure photoemission at the Advanced Light Source, introduces the subject of this technique. Its unique ability to get data about chemical composition of species involved in chemical reactions modeled inside the experimental apparatus under realistic conditions drives numerous applications for studies of catalytic reactions and processes occurring during the generation of energy.

The article by J. Avila and M. C. Asensio describes the first *operational* beamline for nano-ARPES at Synchrotron SOLEIL. Collecting ARPES data from the spot measuring only a few tens of a nanometer enables previously non-feasible studies of extremely small samples and samples with coexisting phases. Development of nano-ARPES has greatly benefited from the improved beam stability of the latest batch of synchrotron rings. The advent of future diffraction-limited synchrotron rings will probably trigger a widespread development of this technique.

The last report comes from the ADRESS beamline at the Swiss Light Source, where a group led by V. Strocov has developed a versatile ARPES instrument using photon en-

Table 1: APXPS instruments at synchrotron radiation facilities (as of January 2014)

Facility	Beamline	Source	Energy range (eV)	Type of spectrometer	Status
Advanced Light Source, Berkeley, CA, USA	9.3.2 9.3.1 11.0.2 11.0.2	Bending magnet Bending magnet EPU EPU	200–800 2000–6000 90–1500 90–1500	Scienta R4000 HiPP Scienta R4000 HiPP-2 Modified Specs Phoibos 150 Specs Phoibos NAP 150	Operational Operational/Roll-up Operational Operational
ALBA, Barcelona, Spain	CIRCE, NAPP, BL24	APPLE II helical undulator	100–2000	Specs Phoibos NAP 150	Operational
BESSY-II, Berlin, Germany	ISISS CAT@EMIL	Bending magnet Undulator	80–2000 80–2000	Specs Phoibos NAP 150 HV	Funded/Operational 2015
Brazilian Synchrotron Light Source, Campinas, Brazil	PGM	Apple II undulator	100–1500	Scienta R4000 HiPP	Operational/Roll-up
Diamond, UK	VERSOX	Bending magnet	200–2800		Funded
MAX-IV, Lund, Sweden	I511 SPECIES HIPPIE	Undulator EPU EPU	50–1500 27–1500 263–2000	Specs Phoibos NAP 150 Specs Phoibos NAP 150	Operational 2010–2013 Operational Funded/Operational 2016
National Synchrotron Light Source, Upton, NY, USA	X1A1 CSX-2	Undulator Undulator	250–850 200–2000	Specs Phoibos NAP 150 Specs Phoibos NAP 150	Operational until 9/2014 Operational from 10/2014
Photon Factory, Tsukuba, Japan	7A 13A	Bending magnet Undulator	100–1500 30–1600	Omicron EA125HP	Operational/Roll-up
Soleil, Gif-sur-Yvette, France	TEMPO	Undulator	50–1200 eV	Specs Phoibos NAP 150	Commissioning/Operational in Fall 2014
Shanghai Synchrotron Radiation Facility, Shanghai, PR China	Ambient pressure spectroscopy beamline	Bending magnet	50–2500		Funded
SPring-8, Hyogo, Japan	36XU 07LSU	In-vacuum type tapered undulator Segmented cross undulator	4500–35000 250–2000	Scienta R4000 HiPP-2 Specs Phoibos NAP 150	Operational Commissioning
Stanford Synchrotron Radiation Light Source, Menlo Park, CA, USA	13.2	Undulator	200–1100	Modified Scienta SES100	Operational
Swiss Light Source, Villigen, Switzerland	SIM Phoenix	Apple II undulator Apple II undulator	150–1800 1500–8000	Scienta R4000 HiPP-2	Operational/Roll-up

SP8

Technical considerations

The main obstacle to performing XPS experiments at elevated pressures is the scattering of electrons in the gas phase. The attenuation of the signal I at pressure p compared to the signal I_0 at pressure p_0 under vacuum conditions is proportional to exp-(σdp), with d the distance that the electrons travel in a gas at pressure p, and σ the scattering cross-section, which depends on the chemical composition of the gas phase. Thus, to minimize the attenuation of the signal, the distance that the electrons travel through the gas phase needs to be limited. In addition, the electron detector and hemispherical analyzer need to be kept under high vacuum ($<10^{-7}$ mbar). Since each differential pumping stage provides pressure differentials of about 10^{-2} to 10^{-5} (depending on aperture size, pumping speed, and type of gas), it follows that several differential pumping stages are needed for pressures in the sample cell in the mbar range. In addition, the X-ray source (e.g., a synchrotron beamline) also needs to be kept under high vacuum. The latter can be achieved through the use of an X-ray transparent window, most commonly a silicon nitride or aluminum membrane (thickness ~100 nm),

AP-XPS systems in the world

Operation

[SR]
ALS BL11.0.2/BL9.3.2
BESSY
SSRL
MAX-lab
NSLS
SOLEIL
PF
SPring-8 BL36XU, BL07LSU
SLS

[Lab]
ISAS, Dortmund
Norte Dam
U. Penn
Mickiewicz Univ.

Construction

[SR]
SOLEIL
ALBA
[Lab]
TU Bergakademie Freiberg
University Leipzig
Flinders Univ.

Planning

[SR]
ELLETRA
Diamond
Shanghai

雰囲気下光電子分光(NAP-XPS)

SPring-8 BL07LSU
高輝度軟X線

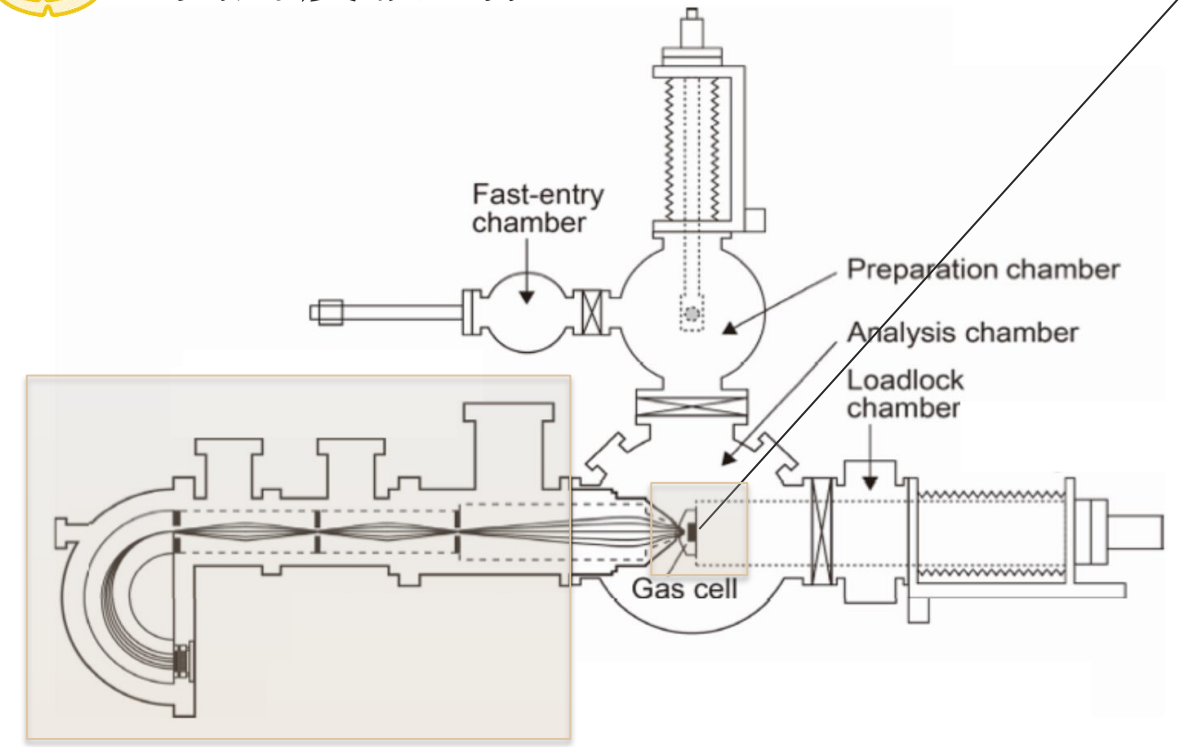

差動排気型アナライザー

ガスセル

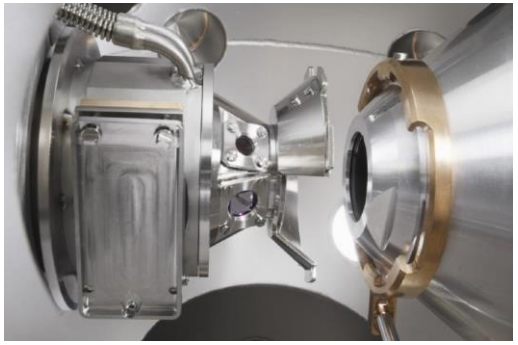

ノズル　φ300 μm

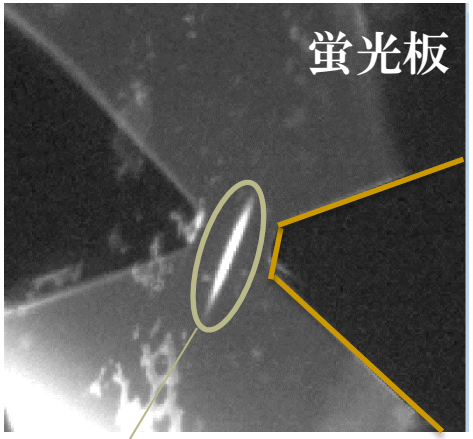

放射光

ガス雰囲気下(<20 mbar)での光電子分光測定を確認